~~Can we gain knowledge on COS~~ Improved understanding of anthropogenic and biogenic ~~emissions~~ carbonyl sulfide (COS) fluxes in Western Europe from ~~a single atmospheric~~ long-term continuous mixing ratios ~~measurement site?~~measurements

Antoine Berchet[1,*], Isabelle Pison[1,*], Camille Huselstein[1], Clément Narbaud[1], Marine Remaud[1,2], Sauveur Belviso[1], Camille Abadie[1], and Fabienne Maignan[1]

[1]Laboratoire des Sciences du Climat et de l'Environnement, CEA-CNRS-UVSQ, Gif-sur-Yvette, France
[2]now at: Faculty of Science, A-LIFE, Vrije Universiteit Amsterdam, 1081 HV Amsterdam, the Netherlands
[*]Correspondance: antoine.berchet@lsce.ipsl.fr, isabelle.pison@lsce.ipsl.fr

Abstract. Lack of knowledge still remains on many processes leading to COS atmospheric fluxes, either natural such as the oceanic ~~emissions~~ sources or the vegetation and soil ~~fluxes~~uptakes, or anthropogenic, with emissions from industrial activities and power generation. Moreover, COS atmospheric mixing ratio data are still too sparse to evaluate the estimations of these sources and sinks at a better scale than the global scale; in this context, regional estimates are very challenging. This study assesses the anthropogenic emissions and biogenic COS ~~fluxes~~uptakes at the regional scale, in the footprint of a measurement site in Western Europe, at a seasonal to diurnal time resolution over half a decade. The continuous time series of COS mixing ratios obtained at the monitoring site of Gif-sur-Yvette (in the Paris area) from August 2014 to December 2019 are compared to simulations with the Lagrangian model FLEXPART, transporting oceanic ~~emissions~~sources, biogenic land fluxes from the ~~process-model ORCHIDEE and~~ land-surface models ORCHIDEE and SiB4 and anthropogenic emissions by two different inventories. The anthropogenic emission inventory based on reported industrial emissions and the characteristics of coal power plants in Europe is consistent with the observations. The flat temporal variability applied to anthropogenic fluxes due to lack of information on industrial and power-generation activity in viscose factories and coal-power plants and the potential mismatches in the representation of the plumes emitted from these hot-spots in the model are the main limitations of this inventory. We find that the net ecosystem COS uptake simulated by ~~ORCHIDEE~~ both ORCHIDEE and SiB4 is underestimated in winter at night, which suggests improvements in the parameterization of the nighttime uptake by plants for COS. In Spring, SiB4 simulates persistent nighttime uptake by vegetation, contrary to ORCHIDEE, which leads to more realistic simulations with SiB4 than with ORCHIDEE. In Summer, both models properly represents fluxes, with better agreement from ORCHIDEE in terms of magnitudes.

1 Introduction

Carbonyl sulfide (COS) is absorbed along CO_2 by plants during photosynthesis. But COS, contrary to CO_2, is almost not emitted during respiration-like processes ~~(Protoschill-Krebs et al., 1996; Montzka et al., 2007; Sandoval-Soto et al., 2005)~~(Protoschill-Krebs et

. This has led to ~~thinking~~ suggestions that COS could be used as a tracer for quantifying and/or reducing uncertainties on CO_2 fluxes due to photosynthesis ~~(Whelan et al., 2018, and references within)~~(e.g., Whelan et al., 2018; Launois et al., 2015; Hilton et al., 2017).

25   The methodology called atmospheric inversion consists in assimilating mixing ratio data into a statistical framework (called Bayesian because it is based on Bayes' theorem) making use of some prior knowledge of sources and sinks and of a chemistry-transport model (CTM) to link fluxes (either emissions to the atmosphere or uptake) to atmospheric mixing ratios, in order to retrieve optimized fluxes. The optimized fluxes are statistically consistent with all the information provided in the prior knowledge of sources and sinks and in the measured atmospheric mixing ratios. The minimum requirements for atmospheric

30   inversion to yield useful insights are therefore *i)* that the CTM resolution, various inputs (such as meteorological fields, flux maps) and physical and chemical parameterizations are relevant to the targeted spatio-temporal scale, so that the link between fluxes and atmospheric mixing ratios does not entail large or poorly characterized uncertainties, but also *ii)* that the uncertainties on the prior knowledge of sources and sinks are well characterized, so that the corrections applied to obtain optimized fluxes are physically meaningful. On top of these general requirements, when using COS mixing ratio data to get information on

35   CO_2 uptake during photosynthesis, the atmospheric inversion must be provided with information that make it possible to disentangle the influence of the biogenic sink of COS from the influence of anthropogenic and other biogenic fluxes on the measured COS mixing ratios. This can be done by providing to the CTM fluxes of COS which are well-known, i.e., with small and well-characterized uncertainties. It is therefore a strong limitation to today's potential use of COS to gain insight into CO_2 photosynthesis fluxes that COS sources and sinks are not very well known so far, with only a few estimations available for the

40   various categories (Whelan et al., 2018; Remaud et al., 2023) , which can be summarized as:

   – the natural oceanic source, due to both direct COS emissions and indirect emissions via dimethyl sulfide (DMS) and carbon disulfide (CS_2) (Mihalopoulos et al., 1992). Note that fresh waters also contribute to COS emissions (Du et al., 2017). In the atmosphere, CS_2 is oxidized into COS in about 10 days (Bandy et al., 1981; Khalil and Rasmussen, 1984; Chin and Davis, 1993; Stickel et al., 1993). The total of direct and indirect oceanic emissions are estimated at

45   265 ± 210 GgS.yr^{-1} by Lennartz et al. (2017) (cited in Whelan et al., 2018) and Lennartz et al. (2021).

   – anthropogenic sources of COS, restricted to particular industries, once again in contrast to CO_2. These anthropogenic sources are due to industries which emit either COS or CS_2. The main source of anthropogenic COS is the oxidation of CS_2 emitted by the viscose industry which includes factories producing viscose as their final product (named hereafter viscose-producing industry) or as the by-product of their main process for producing, e.g., sponges, cellophane (Chen,

50   2015; Water, 2011) (named hereafter viscose processors). Other sources are smaller and emit both COS and CS_2: they are in the sector of energy production with coal use in power plants but also the combustion of oil and bio-fuels (Attar, 1978), the pulp mills due to the kraft process (Brownlee et al., 1995; Cheremisinoff and Rosenfeld, 2010), industries using aluminum oxide electrolysis to produce aluminum (Harnisch et al., 1995), the producers of pigments with carbon black used for tires or the food industry and the widely used white titanium dioxide. For the whole world in the year

55   2012, the inventory by Zumkehr et al. (2018) gives a total of 400±180 GgS.y^{-1} for all anthropogenic emissions (used in the budget elaborated by Whelan et al., 2018).

– besides the anthropogenic combustion of bio-fuels, biomass burning in open fires either natural (e.g., wild fires due to lightning) or human-caused (e.g., agricultural practices) is also a source of COS, estimated at an average 60±37 GgS.y^{-1} by Stinecipher et al. (2019).

60   – soils can also be sources of COS under specific conditions such as high temperature and incoming radiation, related to abiotic production processes (Whelan and Rhew, 2015; Whelan et al., 2016, 2018; Kitz et al., 2017, 2020). The anoxic soil contribution has recently been estimated at 96 GgS.yr^{-1} with the ORCHIDEE process-model (Abadie et al., 2022, see also details on ORCHIDEE in Section 2.2.2).

– the main biogenic sink is due to the uptake of COS by vegetation (Whelan et al., 2018): COS is irreversibly consumed by
65   the carbonic anhydrase enzyme in leaves (DiMario et al., 2016). Soils can also absorb COS due to soil microorganisms that also contain the carbonic anhydrase enzyme (Masaki et al., 2021). The order of magnitude obtained for the uptake by vegetation is -530 GgS.yr^{-1} with the ORCHIDEE process-model (see details on ORCHIDEE in Section 2.2.2), to compare, for example, to -664 GgS.yr^{-1} with the Simple Biosphere Model (SiB4 Kooijmans et al., 2021a). The oxic soils can both produce and consume COS but they are a net sink, estimated recently at -126 GgS.yr^{-1} with the
70   ORCHIDEE process-model (Abadie et al., 2022). The net soil sink (taking into account the source due to anoxic soils and the net sink due to oxic soils) of COS is therefore estimated at -30 GgS.yr^{-1} by Abadie et al. (2022), to compare to, e.g., -89 GgS.yr^{-1} according to SiB4 Kooijmans et al. (2021a).

– the atmospheric sink of COS is due to its oxidation by OH radicals and its photolysis in the stratosphere (estimated respectively at -130 to -80 GgS.yr^{-1} and -50±15 GgS.yr^{-1} by Whelan et al., 2018).

75   Reducing the uncertainties on the estimates of all these sources and sinks at the global scale at as fine temporal and spatial resolutions as would be required to bring information on CO_2 fluxes due to photosynthesis does not seem easy to accomplish in the next few years. The first challenge is the lack of knowledge still remaining on many processes which lead to COS or CS_2 emissions in the atmosphere. For example, Remaud et al. (2023), Ma et al. (2023) and Ma et al. (2021) conclude that a source may be missing in the Tropics (probably from the ocean) and that the uptake of COS by vegetation at high northern latitudes
80   is too small. Some natural processes emitting COS in the atmosphere are still only suspected, for example in plants used in agriculture (Belviso et al., 2022a; Maseyk et al., 2014; Bloem et al., 2012). The second difficulty is the lack of data on COS atmospheric mixing ratios (Montzka et al., 2007), which could be used in CTMs to evaluate the available estimations of sources and sinks at the regional scale, although the National Oceanic and Atmospheric Administration (NOAA) provides atmospheric mixing ratios of COS at several stations, which are useful at the global scale. Still, NOAA data are based on monthly or at
85   best biweekly flask samples, limiting our ability to use them to constrain fluxes at scales smaller than the global to continental scales. Observations with higher frequency are very sparse globally (Belviso et al., 2020; Kamezaki et al., 2023; Zanchetta

et al., 2023; Kooijmans et al., 2016; Commane et al., 2015) and were not yet used for long-term systematic assessment of regional COS fluxes.

To begin to tackle the issue, Belviso et al. (2020) have made use of one of the few continuous time series of COS atmospheric mixing ratios, available in the Paris area, to assess the budget of COS in this area at the seasonal scale and during pollution peaks. Even though the area is almost always a COS sink, local biogenic emission episodes appear in summer and anthropogenic emissions from the Benelux, Eastern France and Germany are occasionally transported so as to influence the area in winter. Belviso et al. (2022b) then tried to use the information brought by the same COS time series of mixing ratios to learn more about the anthropogenic emissions in the footprint of the station, which covers part of Western Europe (including Benelux, Eastern France and Germany) and part of the Atlantic. The relatively long continuous time series made it possible to point to an issue in the oceanic and anthropogenic fluxes in this footprint but not, at this stage, to go further, e.g., characterize accurately or even correct the issue. Following these results, Belviso et al. (2023) used a semi-quantitative approach to assess the gridded inventory of direct and indirect anthropogenic emissions of COS by Zumkehr et al. (2018) in France. The main conclusion of this work is that COS emissions in France are overestimated in this inventory by one order of magnitude and another way of mapping these emissions is required.

Therefore, the present study aims at building a set-up that makes it possible to quantitatively assess the anthropogenic and biogenic COS fluxes at the regional scale, i.e., in the footprint of one measurement site in Western Europe at a seasonal to diurnal time resolution over a period of half a decade. For this, we use the continuous time series of COS mixing ratios measured in the Paris area from summer 2014 to the end of year 2019, as described in Section 2.1. We compare them to the concentrations simulated from marine, biogenic and anthropogenic fluxes in the area of interest (detailed in Section 2.2) combined to the contribution due to the rest of the world (Section 2.1) by the modeling tool described in Section 2.3. After an assessment of the general performances of the model (Section 3.1), we are able to quantitatively evaluate the anthropogenic sources from Western Europe as estimated by Zumkehr et al. (2018) (hereafter referred to as "Zumkehr's inventory") and by our more targeted inventory (Section 2.2.3), confirming discrepancies from Belviso et al. (2023) in Zumkehr's inventory in France in particular, but also in Western Europe in general. Contrary to Belviso et al. (2023), the present study goes one step further by quantitatively assessing discrepancies in Zumkehr's inventory and by proposing a new inventory based on industrial emission declaration in the European Union. Having more reliable anthropogenic emissions, we can inquire into biogenic emissions, which is one of the main original purpose of studying COS. We study the seasonal and diurnal cycles of biogenic fluxes, based on the ORCHIDEE and the biogenic fluxes as simulated by the ORCHIDEE SiB4 processed-based land surface model models (Section 3.3); this allows us to point to strengths and weaknesses in the two models.

2 Data and methods

2.1 Measurements and set-up of background mixing ratios

The measurements used in this study constitute a quasi-continuous time series of COS atmospheric mixing ratios obtained at the monitoring site of Gif-sur-Yvette (GIF) located in the Paris area at 48.7109°N and 2.1476°E at 163 m asl with an inlet

120 height 7 m agl. ~~Gas chromatography is used to measure COS mixing ratios~~A commercial gas chromatograph (Varian 3800) coupled with a cryogenic preconcentrator (ENTECH P7100) for sample preparation, and a mass spectrometer detector (Varian Saturn 2200) for COS detection, were used to analyse this gas, as described by Belviso et al. (2013), Belviso et al. (2016) and Belviso et al. (2020). Calibration is carried out using 1-ppm primary standard, leading to 1.2% precision.

The GIF time series of hourly data spanning from August 2014 to December 2021 is available in Belviso et al. (2022b). In
125 this study, we make use of the time series from August 2014 to December 2019 only (Figure 1, and Fig. A1 to A6), which covers the period of availability of inputs required for simulations, in particular global concentration fields used to compute the background signal (see Section 2.1 and Section 2.3).

The time series of flask measurements sampled by the National Oceanic and Atmospheric Administration (NOAA) network at Mace Head (MHD) in Ireland at 53.3°N and 9.9°W at 42 m asl (described in Montzka et al., 2007, with 1 to 5 pairs of flask
130 per month, collected mostly between 8:00 and 17:00 UTC) are also shown in Figure 1 to illustrate the so-called "background", i.e., the overall contribution of all the sources and sinks which are not in our area of interest. In our study, which focuses on Western Europe and more particularly on the footprint of GIF, the mixing ratios at MHD are representative of the background when the air masses are advected from the West, which is a frequent meteorological configuration (Belviso et al., 2020).

The contribution of the background to the simulated mixing ratios is computed using three-dimensional fields at the global
135 scale. The COS mixing ratio fields used here are obtained from Remaud et al. (2022), at a horizontal resolution of 3.75° in longitude and 1.875° in latitude for 39 pressure levels at a three-hourly time resolution (illustration in Figure 2). They were designed to fit the background NOAA observation sites, such as MHD.

2.2 Fluxes

In the following, "emission" denotes fluxes which are sources as seen from the atmosphere and "uptake" denotes fluxes which
140 are sinks as seen from the atmosphere; "flux" is used for (ensembles of) processes which can be either sources or sinks.

Our simulations, detailed in Section 2.3, take into account COS fluxes in the area of interest as provided by the data sets described here. The contributions from biomass burning emissions and the atmospheric sink are neglected in this study, as well as the emissions from anoxic soils. They play a significant role at the global scale for long-term studies (e.g., Ma et al., 2023), but are negligible compared to ocean emissions (see Sect. 2.2.1), biogenic fluxes (see Sect. 2.2.2) and anthropogenic emissions
145 (see Sect. 2.2.3).

2.2.1 Ocean emissions

The ocean data set designed by Lennartz et al. (2021) and Lennartz et al. (2017) includes direct emissions of COS and indirect emissions of COS via CS_2 and ~~DMS~~ dimethylsulfide (DMS) emissions at a monthly resolution and at a $1° \times 1°$ horizontal resolution~~.~~, respectively. DMS emissions can only be non natural and are expected to have a small impact on COS
150 concentrations after oxidation, however, past work justified negligible impact on overall simulations when not accounting for all DMS emissions (Sarwar et al., 2023; von Hobe et al., 2023).
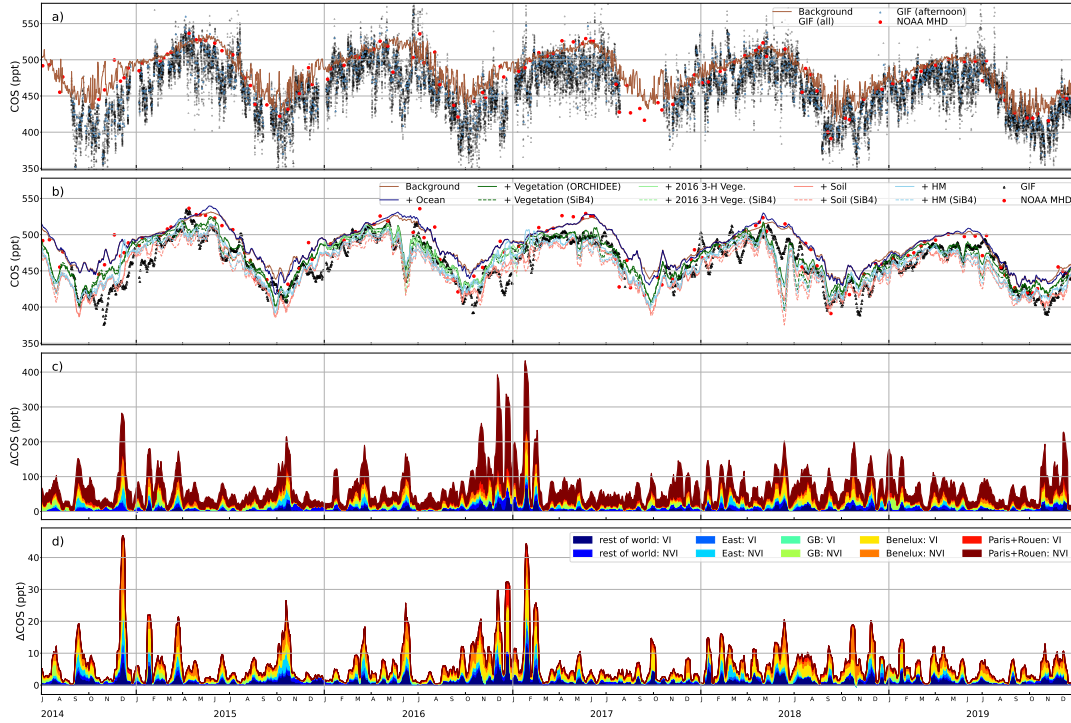
Figure 1. *Time series of observed and simulated atmospheric mixing ratios of COS. a) Hourly COS observations at GIF, with afternoon (12:00-18:00 UTC) averages super-imposed, and flask measurements at Mace Head (MHD) and simulated background described in Section 2.1. Remark: the limits set on the y-axis do not show ≈ 50 extremely low values and ≈ 190 extremely high values of hourly COS observations. b) 10-day rolling mean of GIF afternoon observations, with cumulative simulated contributions from background, ocean sources and biogenic land fluxes (see Section 2.3 for details, "2016 3-H Vege." = 3-hourly vegetation uptake as available for 2016), c) 10-day rolling mean of simulated anthropogenic contributions to COS mixing ratios by region (shown in Figure 2) and sector according to Zumkehr's inventory (see Section 2.2.3, VI = viscose industry, NVI = non-viscose-related emissions), d) 10-day rolling mean of simulated contributions by region (shown in Figure 2) and sector according to our home-made inventory ("HM", see Section 2.2.3, Figure 2). Remark: afternoon data are shown here because the model is assumed to better represent the vertical mixing in the afternoon so that the comparison to measurements highlights the discrepancies in fluxes compared to the model's errors.*

The emissions of the three species have been computed using box models calibrated with ship-borne measurements made in different parts of the globe and result in a data-driven data set for COS oceanic emissions. This ocean data set has been optimized by Remaud et al. (2022) by assimilating NOAA flask data into the model LMDZ. This optimized data-set has been compared to others by Ma et al. (2023) (therein called "OPT-LMDZ") and gives very similar results to other datasets when evaluated with independent atmospheric data at the global scale. Our ocean fluxes give total (direct+indirect) emissions of COS of 507 GgS~~/y~~.yr^{-1} on average over 2014-2019 and 4 GgS~~/y~~.yr^{-1} in our domain of interest.

2.2.2 Biogenic land fluxes

In this study, biogenic land fluxes refer to vegetation uptake and soil exchanges~~and are simulated using the ORCHIDEE land surface model (Krinner et al., 2005). In ORCHIDEE~~. We compare simulations based on the ORCHIDEE (Krinner et al., 2005) and SiB4 (Haynes et al., 2019b, a) land surface models.

In ORCHIDEE and SiB4, a mechanistic representation of vegetation COS uptake has been implemented following Berry et al. (2013), and soil COS exchanges are computed based on the model from Ogée et al. (2016), representing both COS uptake and emission by soils~~(see Maignan et al. (2021) and Abadie et al. (2022) for more details on~~. The representation of biogenic COS fluxes in SiB4 is described in details in (Kooijmans et al., 2021b), while the vegetation and soil ~~models, respectively).~~ COS models in ORCHIDEE are presented in Maignan et al. (2021) and Abadie et al. (2022), respectively.

Monthly variable near-surface COS concentrations are prescribed to compute the biogenic land fluxes in ORCHIDEE and SiB4. These concentrations were simulated using optimized surface COS fluxes in the LMDZ atmospheric transport model and extracted from its first vertical level (Remaud et al., 2022) for ORCHIDEE. Similarly, optimized fluxes from Ma et al. (2021) are transported using TM5 to compute SiB4 fluxes. Biogenic land fluxes are computed with a horizontal resolution of ~~1 degree × 1 degree~~ $1° \times 1°$ at a monthly time-step (illustrated in Figure 2), thus losing any temporal variability at the synoptic scale. The data set used here estimates the average uptakes of COS over 2014-2019 at 22.6 ~~GgS/y~~ GgS.yr^{-1} (resp. 29.8 GgS.yr^{-1}) by the vegetation according to ORCHIDEE (resp. SiB4) and 12.9 GgS~~/y~~.yr^{-1} by the soil in our domain of interest. In particular, biogenic fluxes ~~have~~ exhibit a significant diurnal cycle~~, as COS fluxes are relative to photosynthesis occurring during day-time only~~. Indeed, vegetation COS uptake is regulated by stomatal conductance. There is a residual uptake during nighttime due to incomplete stomatal closure, and a stronger uptake during daytime when stomatal conductance increases. We assess the sensitivity of our simulations to daily varying biogenic fluxes by using 3-hourly vegetation uptake as simulated by ORCHIDEE and SiB4 for the year 2016. The ~~difference performance of our model~~ different performances of the models with monthly and 3-hourly fluxes is evaluated in Sect. ~~3.1~~3.3.

2.2.3 Anthropogenic emissions

Two different COS anthropogenic inventories are used in this study. The inventory by Zumkehr et al. (2018) accounts a total of 62.1 GgS.yr^{-1} in the domain of interest, compared to our more realistic inventory, with a total of 11.2 GgS.yr^{-1}.

Main characteristics of Zumkehr's inventory

The inventory by Zumkehr et al. (2018) accounts for the sectors emitting the most COS and CS_2 at the country level and provides yearly emissions from 1980 to 2012. Here, the values for the year 2012, as the most recent available, have been used. In our domain of interest, they amount to a total of 62.1 GgS.yr^{-1} among which 20.5 GgS.yr^{-1} for the viscose industry, 14.5 GgS.yr^{-1} for coal use, 23.6 GgS.yr^{-1} for the pigments and 2.8 GgS.yr^{-1} for aluminum production. The sub-country distribution is done according to secondary proxies, such as energy industry activity or industrial CO_2 emissions. This proxy-based distribution proved efficient in the U.S., but can be misleading in some European countries. For example, in France, ~~where coal-based energy production is almost absent and where viscose industry is limited to a handful of site~~only one power plant is fueled by coal, and only a very few viscose sites are still active, no necessarily near the biggest cities in the country. On the opposite, Zumkehr's methodology leads to a distribution of national emissions ~~to many hot spots close to~~ around the main urban areas, decorrelated to real emissions. As shown in Figure 2 and Fig. 1c of Belviso et al. (2023), such a hot spot appears in the Paris area, with its center located close (about 20 km) to the North-East of GIF.

In the following, the sectors provided in Zumkehr's inventory (Zumkehr et al., 2018, therein Tab 1) are grouped as viscose industry emissions (abbreviated as "VI"), which include the sectors named "Pulp & Paper", "Rayon Staple", "Rayon Yarn", and non-viscose-related emissions (abbreviated as "NVI"), which include the sectors named "Agricultural Chemicals", "Aluminum Smelting", "Carbon Black", "Industrial Coal", "Residential Coal", "Industrial Solvents", "Titanium Dioxide (TiO2)", and "Tires". Maps and bar plots for selected European countries are available in Belviso et al. (2023) main text and supplementary material.

Home-made inventory

To overcome the caveats of Zumkehr's inventory in Western Europe, we designed our own inventory, following the conclusions of Belviso et al. (2023), and based on:

– explicit declaration of CS_2 emissions from the viscose industry (including rayon yarn and staple and other products such as cellulosic casings) with a comprehensive list of plants in Europe (abbreviated as "VI" and comparable to the VI emissions in Zumkehr's inventory) for the year 2018 (available at the time of the study); see details in ~~Tab.~~Tables 2-3 of Belviso et al. (2023). The total emissions in our domain of interest are ≈ 4.7 GgS~~/y~~.yr^{-1} in 2018.

– for coal, CO_2 emissions for all coal power plants in Europe (from the Global Energy Monitor's Global Coal Plant Tracker) were used to estimate COS emissions for each year based on a unique emission factor (abbreviated as "NVI" and comparable to the NVI coal-related emissions in Zumkehr's inventory). We used a value of 5.7×10^{-6} molecules of COS emitted for each molecule of CO_2 during coal combustion. The average emissions over 2014-2019 are ≈ 6.5 GgS~~/y~~.yr^{-1} in our domain of interest.

Through lack of data, we did not apply any temporal profiles to viscose and coal emissions, even though they are expected to strongly vary over the year, even from one week to the next one. For viscose, we applied no inter-annual variability and keep

215 emissions stable based on the year 2018. For coal emissions, inter-annual variability is based on yearly CO_2 emission values. Compared to Zumkehr's inventory, ours (Figure 2) displays only a few hot spots of emissions in France: 4 viscose industry sites with big factories and 4 coal-burning power plants. The closer to GIF is in the city of Beauvais, which lies about 85 km to the North of GIF, i.e., further than the Paris area.

2.3 Simulations of concentrations

220 The modelled COS mixing ratios were obtained by using the Lagrangian atmospheric transport model FLEXPART (FLEXible PARTicle) version 10.3 (Stohl et al., 2005; Pisso et al., 2019). The model FLEXPART is driven by meteorological data from the European Centre for Medium-range Weather Forecast (ECMWF) ERA5 (Hersbach et al., 2020) with 3-hourly intervals and 60 vertical layers, retrieved using the FLEX-extract toolbox (Tipka et al., 2020). In our case, meteorological data is provided to FLEXPART at a $1°$ horizontal resolution. For the whole duration of the observation period, 2000 virtual particles are released 225 every 6 h and followed backward in time for 10 days. The multiple FLEXPART simulations are driven by the GUI-based toolbox designed by Berchet et al. (2023).

We assume a conversion of CS_2 to COS with a maximum of 87% molar conversion rate, as ~~estimated by Barnes et al. (1994) and as~~ used by Zumkehr et al. (2018). The kinetics of the conversion is approximated by prescribing a half-life of 3 days to CS_2 in the atmosphere. The amount of COS created from a CS_2 source along the transport path of the air mass is then given as 230 $0.87 \times \left(1 - e^{-\frac{t}{\tau n2}}\right)$ with $\tau = 3$ days.

~~So called~~ So-called source-sensitivity (or footprint) maps (Seibert and Frank, 2004) are computed for every release date by counting the number of particles transported above a certain point below a threshold of 500 m above ground level. Source contribution by process-type are inferred by convolving source-sensitivity maps with flux maps from the ocean emissions, the biogenic fluxes and one of the two anthropogenic emission inventories (see Section 2.2.1, Section 2.2.2, Section 2.2.3). One 235 FLEXPART simulation is run for each process or sector and region of interest (see Figure 2) so that the simulations (Table 1) can be combined to include or exclude particular sectors and/or particular regions when building the footprint maps.

The background mixing ratios (Fig. 2f) are calculated by combining the 3D source-sensitivity fields (e.g., Thompson and Stohl, 2014; Pisso et al., 2019) at the end of the backward trajectories with the available COS concentration field (see Section 2.1). The background thus obtained represents the average of the mixing ratios in the grid cells where each particle 240 trajectory terminated 10 days before the observation. For instance, as illustrated in Fig. 2f, for the given date, GIF observations are sensitive to background mostly in North-Western Atlantic (higher sensitivity for deep red contours). The computation of COS contributions from surface fluxes and the background was carried out using the Community Inversion Framework (CIF; Berchet et al., 2021).
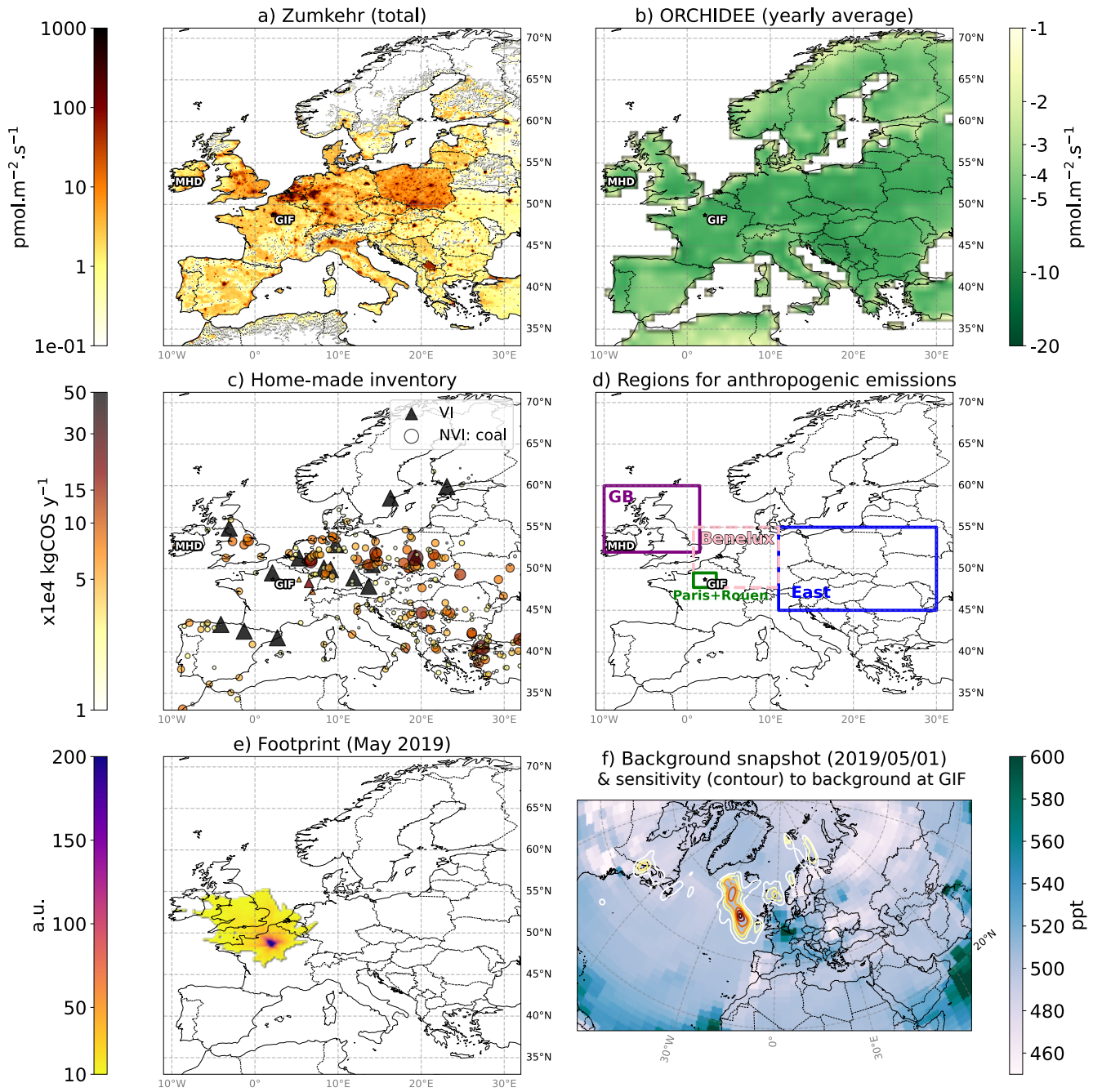
Figure 2. *Maps of input data sets used in our study. a) Zumkehr's yearly, i.e., 2012 total emissions, b) 2019 yearly average biogenic land fluxes from the ORCHIDEE model, c) emission points from viscose and coal industries as defined using our methodology (see Section 2.2.3 for details, here year 2019 for illustration), d) regions of interest for anthropogenic emissions, e) illustration of footprint summed-up over one month, f) snapshot of background concentration fields; contours highlight the computed sensitivity to the background 10-days before observation at GIF (see Sect. 2.3 for details). Remark: units for area (gridded) emissions are pmol.m^{-2} whereas emissions by point sources are in mass units; footprints are shown in arbitrary units (a.u.).*

Fluxes from / Region	ocean	biogenic land	Zumkehr's VI	Zumkehr's NVI	home-made VI	home-made NVI
whole area of interest	o	bl				
Benelux ("B")			ZviB	ZnviB	HMviB	HMnviB
Paris+Rouen area ("U")			ZviU	ZnviU	HMviU	HMnviU
area of interest excluding Benelux and the Paris+Rouen area			ZviW	ZnviW	HMviW	HMnviW

Table 1. *FLEXPART simulations per region (shown in Figure 2) and sector. Each cell: a group of letters indicate that the simulation is run; the same IDs are used for each violin plot in Figure 3. "Z" = Zumkehr's inventory, "HM" = home-made inventory (this study), "VI" or "vi" = viscose industry, "NVI" or "nvi" = non-viscose-related (actually coal-related only in HM, see Section 2.2.3), "U" = Paris+Rouen area = an urban and industrial area, "B" = Benelux, "W" = whole area excluding "B" and "U".*

3 Results and discussion

245 3.1 General performances of the model at GIF

By design, the background contribution (Section 2.1) fits the main monthly variations as measured at a background station such as MHD (Figure 1 a) and b)). Its contribution at GIF ensures a good simulation of the variability (Table 2: Pearson's correlation ≥ 0.75) and a small mean error (RMS ≤ 35 ppt) over the whole period of interest. As expected, adding the natural emissions from the ocean (Section 2.2.1) and the biogenic land fluxes (Section 2.2.2) reduces the bias (by almost 15 ppt in absolute value) 250 and the mean error is decreased by more than 20%.

As mentioned in Sect. 2.2.2, we assess the impact of using temporally resolved biogenic fluxes on our simulations. Making use of a vegetation uptake with a 3-hourly time resolution (during only the year 2016, see Section 2.2.2) does not improve the statistical fit of the model to the observations: the bias and RMS are almost unchanged and the correlation is decreased (Table 2: from 0.74 to 0.72). The variability is not better reproduced when adding the natural emissions to the background (correlation 255 from 0.76 to 0.74, excluding the case of the 2016 3-hourly varying vegetation uptake), which may be due to ~~too coarse a~~ a too coarse variability for the ocean emissions (with a monthly resolution, Section 2.2.1) and an issue with the variability of the vegetation uptake or the soil exchanges, probably at the seasonal scale, which is assessed in Section 3.3. The limited impact, and even degradation, of performances when using the diurnal cycle of biogenic flux suggests an issue in their representation in ORCHIDEE, maybe in the residual ecosystem (vegetation and soil) COS flux simulated at night.

260 The contributions of the anthropogenic emissions by Zumkehr degrades all three indicators of the fit to the measured concentrations at GIF: the bias and mean error are very high (both $\geq$100 ppt), the variability is not reproduced anymore. The regional anthropogenic emissions located in the Paris+Rouen area explain the major part of the discrepancies between the simulation and the measurements (Table 2). According to Zumkehr's inventory, COS emissions in Île-de-France, i.e., the Paris area itself, are mostly ($\approx$62%) due to viscose industry, which is not consistent with the lack of any such factory declaring emissions in this

Contribution	bias (ppt)	RMS (ppt)	corr
Background	23	33	0.76
Background + ocean	23	33	0.75
Background + biogenic land	-5	25	0.73
Background + biogenic land with 2016 3-hourly vegetation	-5	26	0.71
Background + ocean + biogenic land	-5	25	0.74
Background + ocean + biogenic land with 2016 3-hourly vegetation	-4	26	0.72
Background + anthro. Zumkehr	100	151	0.11
Background + anthro. Zumkehr w/o Paris/Rouen	58	87	0.27
Background + coal (HM)	26	35	0.73
Background + viscose (HM)	25	34	0.74
Background + coal (HM) + viscose (HM)	27	37	0.71
Background + ocean + biogenic land + anthro. Zumkehr	72	129	0.14
Background + ocean + biogenic land + anthro. Zumkehr w/o Paris/Rouen	29	66	0.33
Background + ocean + biogenic land + coal HM + viscose HM	-1	25	0.74

Table 2. *Statistical indicators of the performances of the model compared to the daily afternoon (12:00-18:00 UTC) means of measurements at GIF for each contribution; indicators are computed over the whole period when measurements are available, i.e., Aug. 2014 - Dec. 2021. Bias = mean difference model minus measurement; RMS = root mean square model minus measurements; corr = Pearson's correlation coefficient between model and measurement time series. HM indicates emissions from our home-made inventory (see Section 2.2.3).*

265   region. The small (<1%) contribution by coal-using industry is not consistent with the last coal power-plant in the area being closed in 2012. Maybe due to the same type of incomplete information or lack of relevant proxy, the overall European COS emissions in Zumkehr's inventory may be overestimated, as suggested by the very high contributions (more than 100 ppt) due to anthropogenic emissions alone simulated at GIF (Figure 1c).

The contribution of the anthropogenic emissions from our home-made inventory increases the bias and mean error compared
270   to the contributions of the background and natural fluxes only (Table 2). The maximum simulated contributions are between 40 and 50 ppt for some months (Figure 1 c and d), i.e., 10 times smaller than with Zumkehr's inventory. Therefore, the bias and mean error computed over the whole period using our inventory remain more than twice smaller than with Zumkehr without the emissions of the Paris+Rouen area. This order of magnitude is more consistent with the expected anthropogenic contribution required to match the measured concentrations above the background at GIF. Overall statistics are very similar when using
275   only viscose or coal, or both. Further investigation are needed to narrow the range of anthropogenic fluxes in Europe. However, as anthropogenic contributions are observed as peaks, the magnitude of which is difficult to reproduce in transport models, a combination of several observation sites would be needed.

The information which can be retrieved from the time series of concentrations in one measurement site on the relevancy of our inventory compared to Zumkehr's is discussed in the following in terms of activity sectors and source regions.

3.2 Anthropogenic emissions

The general performances of the model at GIF (Section 3.1) show that the total emissions of Zumkehr's inventory lead to a large overestimation of COS concentrations at GIF (Table 2), almost half of which is due to the emissions located in the areas of Paris and Rouen. We represent in Figure 3 the distributions of observations and simulations from different sectors as violin plots. Above the overestimation due to the "natural" contributions, Zumkehr's inventory leads to a median overestimation of ≈52 ppt (Figure 3, "Z total" vs "natural"). The non-viscose-related emissions in the Paris and Rouen areas explain almost half of this discrepancy (24 ppt, "Z total" vs "ZviW + ZnviW + ZviB + ZnviB + ZviU"). The non-viscose-related emissions in "the rest of the world", i.e., the whole world excluding the Paris and Rouen areas and the Benelux explain a bit less than a quarter of the overestimation (12 ppt, "ZviW + ZnviW" vs "ZviW" vs "natural"). Of the remaining 12 ppt, 8 ppt are due to viscose industry emissions in the rest of the world and 1.5 ppt to viscose industry emissions in the Benelux alone. The unrealistic COS emissions in the Paris and Rouen areas not only lead to too high median contributions but also to a large number of high concentration peaks, as shown by the upper elongation of the violin "Z total" (maximum actually > 1995 ppt). As expected, our home-made inventory is more compatible with the observations in GIF (Figure 3). In this case, the background and the oceanic and biogenic land fluxes contribute for ≈40% to the median overestimation (≈4 ppt, Figure 3: "GIF obs" vs "natural") of the observations, compared to 60% for the home-made anthropogenic emissions (≈7 ppt, Figure 3: "HM total" vs "natural"). The distribution of extreme events, i.e., with very high or very low COS concentrations obtained with our home-made inventory is closer to the observed one (Figure 3, upper and lower elongations of "GIF obs" vs "Z total" vs "HM total").

Additional continuous observation sites would be needed in different places of Europe to clarify the relevancy of our inventory beyond the Paris area and vicinity.

3.3 Biogenic land fluxes

Disentangling the main contribution of mismatches between observations and simulations is very challenging with one site only. Differences at the synoptic scale, as represented in Figure 1, can originate from erroneous background, transport discrepancies, or from incorrect fluxes. Still, as represented in the time series in Appendix A, fine scale temporal variability, corresponding to the diurnal cycle, is well reproduced during some periods of the year, especially in Spring. The diurnal cycle is dominated by local influences, with remote influence of the background and of distant fluxes transported to GIF filtered out. We therefore focus here on 12-hour day/night differences in measured or simulated COS concentrations, defined as either "daytime variation" between day D at 6‑p.m. and day D at 6‑a.m. or "nighttime variation" between day D+1 at 6‑a.m. and day D at 6‑p.m.. Thus, these differences are mostly influenced by a combination of small scale meteorological conditions (mostly the diurnal cycle of the planetary boundary layer) and of regional fluxes (within the transport footprint around the station). In the present analysis, we assume that all discrepancies are attributable to fluxes, even though the diurnal cycle of transport in FLEXPART is imperfect. Discrepancies in the diurnal cycle of transport patterns would only impact on the magnitude of the day/night differences, but not on the overall patterns discussed below, thus not impacting our qualitative conclusions.
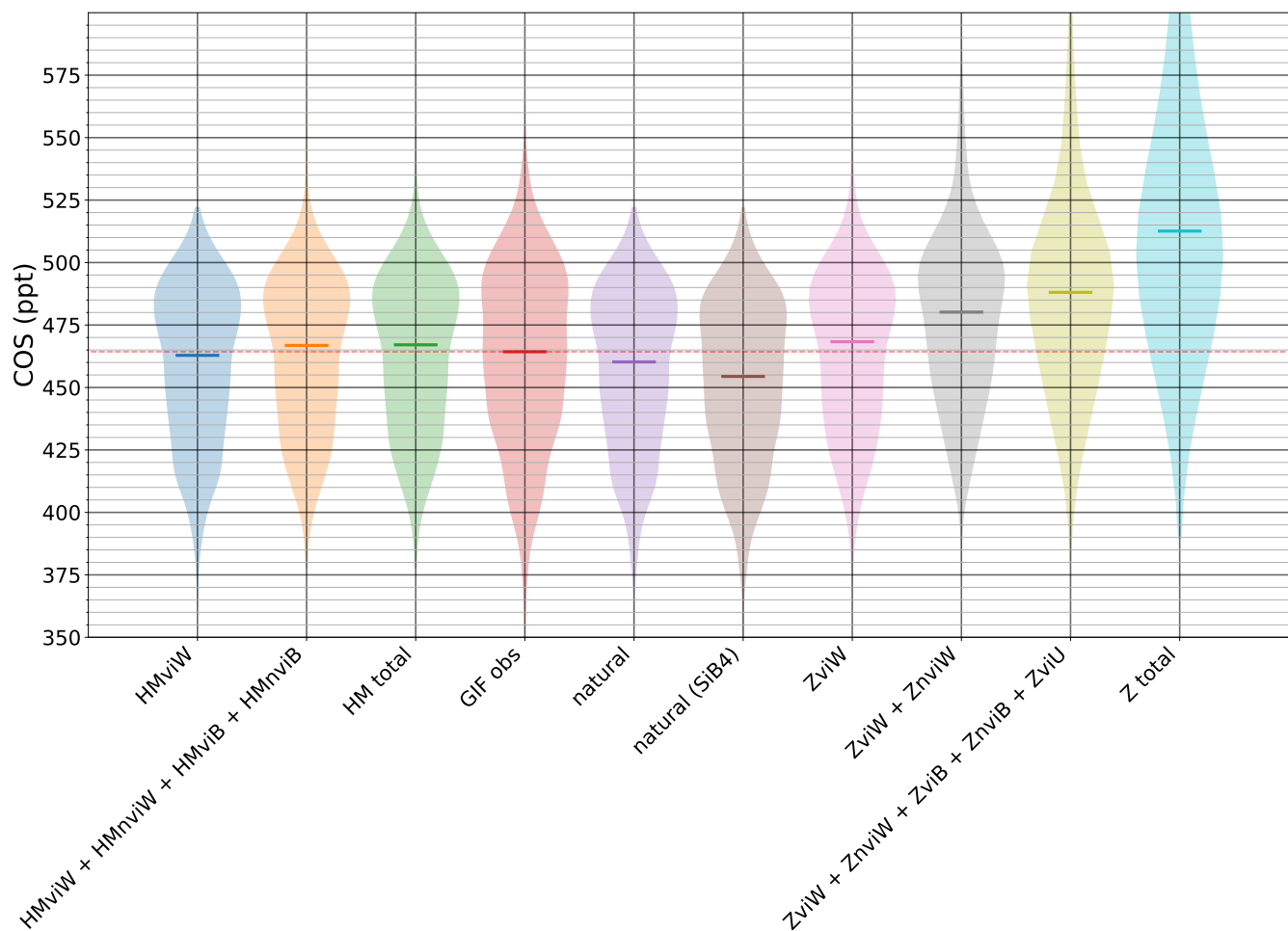
Figure 3. *Violin plots of COS mixing ratios at GIF (solid horizontal lines show the medians) for observations ("GIF obs") and various simulations taking into account different sets of contributions. See Table 1 for the available simulations per region and per sector; "natural" = background + o + bl; "Z total" = natural + ZviW + ZnviW + ZviB + ZnviB + ZviU + ZnviU; "HM total" = natural + HMviW + HMnviW + HMviB + HMnviB + HMviU + HMnviU.*
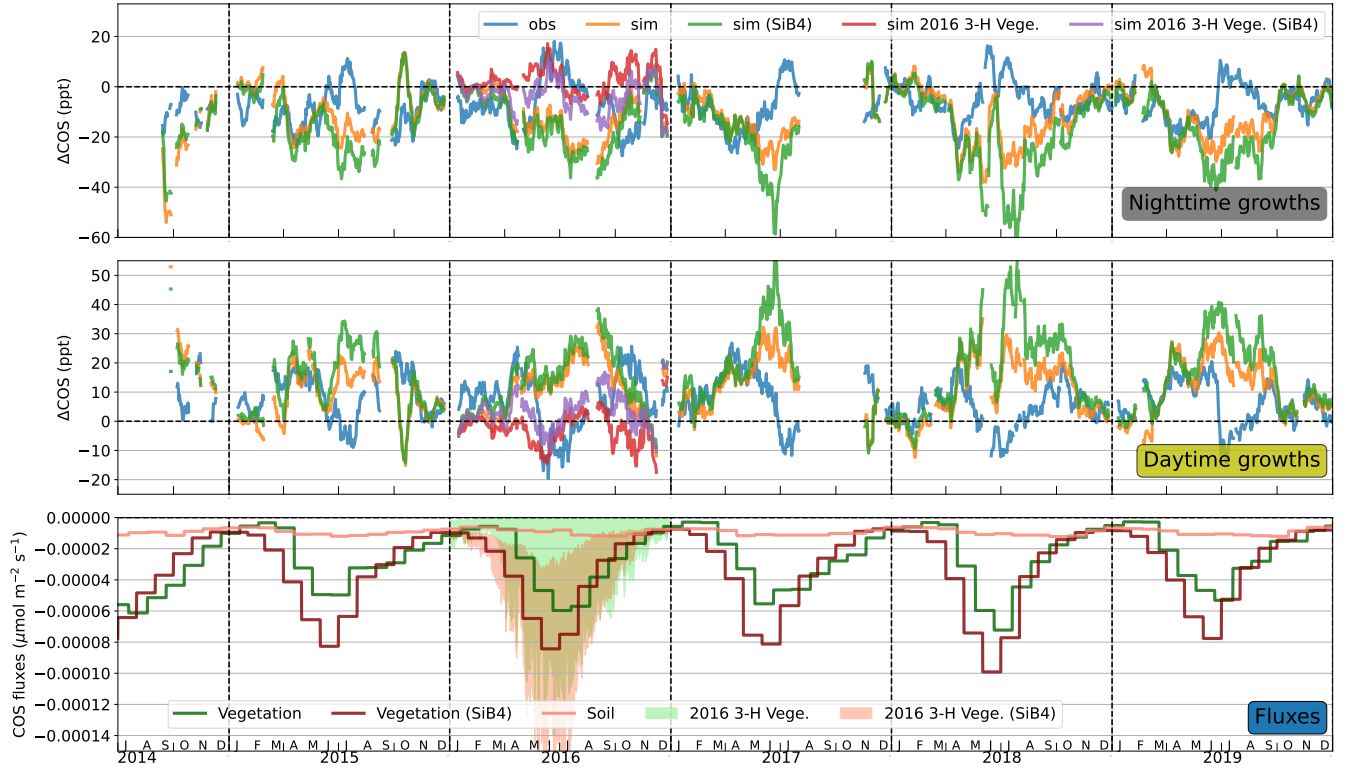
Figure 4. *15-day rolling mean of the nighttime (top) and daytime (middle) variations of the observed and simulated COS concentrations at GIF with matching COS total uptake by vegetation and soils in the domain of interest. Nighttime variation = $[COS]_{D@06:00} - [COS]_{D-1@018:00}$, daytime variation = $[COS]_{D@18:00} - [COS]_{D@006:00}$ (see text for more details); contributions taken into account in the simulations are the background + ocean + our home-made anthropogenic inventory + either biogenic land with a monthly time-resolution ("sim") or biogenic land with 2016 3-hourly time-resolution for vegetation ("sim 2016 3-H Vege."); fluxes are uptakes by the soil, the vegetation at a monthly ("Vegetation") or 3-hourly ("2016 3-H Vege.") resolution (see Section 2.2 for details).* *15-day rolling mean of the nighttime (top) and daytime (middle) variations of the observed and simulated COS concentrations at GIF with matching COS total uptake by vegetation and soils in the domain of interest, using the models ORCHIDEE and SiB4 (see Section 2.2 for details). Nighttime variation = $[COS]_{D@06:00} - [COS]_{D-1@018:00}$, daytime variation = $[COS]_{D@18:00} - [COS]_{D@006:00}$ (see text for more details); contributions taken into account in the simulations are the background + ocean + our home-made anthropogenic inventory + either biogenic land with a monthly time-resolution ("sim") or biogenic land with 2016 3-hourly time-resolution for vegetation ("sim 2016 3-H Vege."); fluxes are uptakes by the soil, the vegetation at a monthly ("Vegetation") or 3-hourly ("2016 3-H Vege.") resolution (see Section 2.2 for details).*

The variations of the nighttime and daytime variations over the available 5.5 years of observation are represented in Figure 4, alongside COS fluxes from regional vegetation and soils, using both the ORCHIDEE and SiB4 models. The observed seasonal cycle of night and day-time variations is similar for all years. The observed nighttime variations are slightly negative in winter (JFM; -7 ppt) then strongly negative in spring (AMJ; -10 ppt) with yearly peaks of ≈ -20 ppt; then, summer positive peaks of 10–15 ppt in July are followed by another negative low in fall (-8 ppt). The positive nighttime variations in summer are most probably due to emissions by the crops, such as rapeseed (Belviso et al., 2022a). Observed day-time variations are opposite with slightly different magnitudes.

In winter (JFM), the vegetation is mostly inactive ~~in ORCHIDEE~~, and soils are at their lowest sink activity with the net soil uptake becoming larger than the vegetation uptake. Thus the contribution of the uptake by the vegetation and soils in our simulations in both ORCHIDEE and SiB4 for both time-resolutions (monthly or 3-hourly) is very small. Both the simulated variations are therefore close to zero (on average, -2 ppt for nighttime and $+1$ ppt for daytime), contrary to observed variations (-7 ppt for nighttime and $+7$ ppt for daytime). This suggests under-estimated COS uptakes at night in winter in ORCHIDEE and SiB4 vegetation and/or soil datasets.

During spring (AMJ), vegetation COS uptake is activated in ORCHIDEE and SiB4. When using constant monthly fluxes with no diurnal cycle, their contribution to the simulated nighttime uptake leads to lower concentrations at night compared to daytime, consistently with observations. In contrast, daytime concentrations are the result of compensating vegetation uptake and mixing in the boundary layer. However, the use of ~~a more realistic~~ 3-hourly vegetation uptake by ORCHIDEE daily cycle results in simulated nighttime and daytime variation close to zero, not consistent with the observations, most likely related to absent uptake at night in ORCHIDEE. In contrary, in SiB4, persistent uptake occurs at night, leading to more realistic simulation than with ORCHIDEE. This discrepancy suggests a persistent nighttime uptake not adequately represented by ORCHIDEE's diurnal cycle, primarily based on photosynthesis uptake. Refining the model ORCHIDEE to improve the representation of nighttime processes may enhance its ability to reproduce observed dynamics, compared to SiB4. Summer (JAS) shows opposite behavior compared to ~~spring~~ Spring, with positive nighttime enhancements. These enhancements are not properly reproduced by both ORCHIDEE and SiB4 when using constant monthly fluxes. With 3-hourly fluxes, both models perform well in Summer. Using a realistic diurnal cycle is key to reproducing the positive nighttime and negative daytime variations. The magnitude of fluxes in ORCHIDEE seems to be in better agreement with observations than with SiB4

During fall (OND), the performance of our simulations exhibits variability across different years, regardless of the inclusion of a vegetation diurnal cycle. Notably, the simulations for the years 2016 and 2017 show significant discrepancies, whereas the results for the remaining four years align well with observational data. This disparity underscores the challenges associated with accurately reproducing the timing of vegetation senescence, particularly given the influence of intricate synoptic meteorological conditions on both vegetation dynamics and the performance of the transport model. The complexity of these interactions poses a significant hurdle in achieving consistent simulation outcomes across all years.

4 Conclusions

The present study analyzes 5.5 years of quasi-continuous COS measurements from the site GIF in the Paris region. Through systematic comparison of measurements with simulations using backward trajectories computed with the Lagrangian model FLEXPART, we provide a quantitative assessment of natural and anthropogenic COS fluxes in Western Europe.

Regarding industrial-emitted COS, we highlight the unrealistic magnitude of anthropogenic fluxes as provided by Zumkehr's inventory (Zumkehr et al., 2018) in Europe. In particular, Zumkehr's inventory suggests very high emissions in the Paris area, inconsistent with the absence of any coal power plant and major viscose industry in the region. We propose another inventory based on declared industrial emissions as well as coal power plants in Europe. The new inventory proves much more consistent with observations and includes only a limited number of emission hotspots in France. Still our inventory comes with several limitations. First, it takes into account the emissions as declared by the "industries"; this category includes only sources above a legally binding threshold. Therefore, we do not account for sources which are under the threshold and we assume them to be small compared to the declared ones; but their overall magnitude remains actually unknown. Second, another limitation arise from the flat temporal variability applied to anthropogenic fluxes in our inventory (similarly to Zumkehr et al., 2018) due to the lack of information on industrial and power-generation activity in viscose factories and coal-power plants. This is expected to be a critical limiting factors as coal-power plant activity depends on energy demands, and viscose industry activity are often organized by batches with days of intense emissions followed by periods with limited emissions. Third, we apply a single emission factor between CO_2 and COS emissions from coal-power plants, whereas this factor depends on the coal used in the combustion, as well as the overall properties and technologies used in the power-plant. Last, limitations are also due to the model-based approach of our study. The sources of COS or its precursors are stacks of factories or power plants, i.e., hot-spots: high sources localized in a very small area compared to the resolution of the chemistry-transport model used to simulate the concentrations. Therefore, the plumes emitted from these hot-spots are not always well represented by the model, depending on the meteorological situation. For hot-spots close to the measurement site (e.g., from the Beauvais region 50 km North of GIF where viscose factories are active), the numerical diffusion of the plumes of COS represented in the model leads most of the time to underestimating simulated concentrations; in particular events, if the error on the wind direction is large enough, the plume may be unduly directed to the site in the model, which leads to overestimating the simulated concentrations. Overcoming the above-mentioned limitations in assessing anthropogenic emissions would mostly need additional observation sites in the region (e.g., Zanchetta et al., 2023, in the Netherlands) to cross-validate our results.

Regarding soil and vegetation fluxes, we are able to suggest that the net ecosystem COS uptake simulated by ~~ORCHIDEE~~ both ORCHIDEE and SiB4 is underestimated in winter at night, requiring improvements in the nighttime processes in land-process models. Even when using ORCHIDEE's vegetation and soil uptakes with a diurnal cycle at a 3-hourly resolution, the analysis of the simulated diurnal cycle of COS concentrations confirms that a night-time uptake is not adequately represented by ORCHIDEE, maybe due to the parameterization of the nighttime uptake by plants for COS. On the opposite, SiB4 has a more realistic representation of Spring diurnal cycles of fluxes with persistent uptake at night, leading to better agreement between simulations and observations of concentrations. In Summer, the magnitude of fluxes by ORCHIDEE is

more consistent than SiB4 fluxes when comparing to observations. Further work is needed to properly compare ORCHIDEE and SiB4 using day/night differences as the model FLEXPART is imperfect in the representation of the diurnal cycle of transport and dispersion. Replicating our study with another transport model and other meteorological constraints would allow to assess the uncertainty on diurnal simulations, even these uncertainties would only impact the magnitudes of the simulations and not there patterns, hence leading to unchanged conclusions.

Although it is based on only one site, the present study provides sufficient elements to identify discrepancies in COS emission data bases and land-process models in Western Europe, due to incorrect parameterizations of fluxes, or missing processes. Still, our single-site study is not sufficient to overcome those discrepancies to reach the level of precision needed to use COS observations as a proxy of plant uptake. A full network of observation sites, analog to the Integrated Carbon Observatory System ~~(ICOS, Ramonet et al., 2011)~~(ICOS; Ramonet et al., 2011), would be a requirement to better quantify anthropogenic fluxes and thus to fully use COS for assessing CO_2 uptake by photosynthesis.

Code and data availability. GIF data is available from https://doi.org/10.14768/6800b065-dcec-4006-ada5-b5f62a4bb832. The CMIP6 version of the ORCHIDEE model including the vegetation and soil COS submodels is available upon request to the authors. Optimized COS concentration fields at the global scale by Remaud et al. (2023) are available at https://zenodo.org/records/7632737 (OPT-LSCE).

Author contributions. AB designed and ran the simulations, including formatting of the home-made emission inventory and of observations; IP and AB analyzed the results, based on preliminary work by CH; CN and CH computed the FLEXPART simulations on which the analysis is based; MR provided the global COS inversions used to determine the background; SB provided the observations at GIF and the home-made French inventory of point sources; CA and FM provided ORCHIDEE fluxes; all co-authors contributed to writing the text.

Competing interests. The authors declare no competing interests relative to the present study.

Acknowledgements. This research has been supported by the 4C project of the European Commission's Horizon 2020 framework programme (Grant 821003). This study was partially funded by the CO2 Human Emissions (CHE) project, which received funding from the European Union's Horizon 2020 research and innovation programme under Grant 776186. Calculations were performed using the resources of LSCE, maintained by J. Bruna and the LSCE IT team.

References

Abadie, C., Maignan, F., Remaud, M., Ogée, J., Campbell, J. E., Whelan, M., Kitz, F., Spielmann, F., Wohlfahrt, G., Wehr, R., Sun, W., Raoult, N., Seibt, U., Hauglustaine, D., Lennartz, S., Belviso, S., Montagne, D., and Peylin, P.: Global modelling of soil carbonyl sulfide exchanges, Biogeosciences, 19, 2427, https://doi.org/10.5194/bg-19-2427-2022, 2022.

405 Attar, A.: Chemistry, thermodynamics and kinetics of reactions of sulphur in coal-gas reactions: A review, Fuel, 57, 201–212, https://doi.org/10.1016/0016-2361(78)90117-5, 1978.

Bandy, A. R., Maroulis, P. J., Shalaby, L., and Wilner, L. A.: Evidence for a short tropospheric residence time for carbon disulfide, Geophysical Research Letters, 8, 1180–1183, https://doi.org/10.1029/GL008i011p01180, _eprint: https://onlinelibrary.wiley.com/doi/pdf/10.1029/GL008i011p01180, 1981.

410 Barnes, I., Becker, K. H., and Patroescu, I.: The tropospheric oxidation of dimethyl sulfide: A new source of carbonyl sulfide, Geophysical Research Letters, 21, 2389–2392, https://doi.org/10.1029/94GL02499, _eprint: https://onlinelibrary.wiley.com/doi/pdf/10.1029/94GL02499, 1994.

Belviso, S., Schmidt, M., Yver, C., Ramonet, M., Gros, V., and Launois, T.: Strong similarities between night-time deposition velocities of carbonyl sulphide and molecular hydrogen inferred from semi-continuous atmospheric observations in Gif-sur-Yvette, Paris region, Tellus

415 B: Chemical and Physical Meteorology, 65, https://doi.org/10.3402/tellusb.v65i0.20719, 2013.

Belviso, S., Reiter, I. M., Loubet, B., Gros, V., Lathière, J., Montagne, D., Delmotte, M., Ramonet, M., Kalogridis, C., Lebegue, B., Bonnaire, N., Kazan, V., Gauquelin, T., Fernandez, C., and Genty, B.: A top-down approach of surface carbonyl sulfide exchange by a Mediterranean oak forest ecosystem in southern France, Atmospheric Chemistry and Physics, 16, 14 909–14 923, https://doi.org/10.5194/acp-16-14909-2016, publisher: Copernicus GmbH, 2016.

420 Belviso, S., Lebegue, B., Ramonet, M., Kazan, V., Pison, I., Berchet, A., Delmotte, M., Yver-Kwok, C., Montagne, D., and Ciais, P.: A top-down approach of sources and non-photosynthetic sinks of carbonyl sulfide from atmospheric measurements over multiple years in the Paris region (France), PLoS ONE, 15, e0228 419, https://doi.org/10.1371/journal.pone.0228419, 2020.

Belviso, S., Abadie, C., Montagne, D., Hadjar, D., Tropée, D., Vialettes, L., Kazan, V., Delmotte, M., Maignan, F., Remaud, M., Ramonet, M., Lopez, M., Yver-Kwok, C., and Ciais, P.: Carbonyl sulfide (COS) emissions in two agroecosystems in central France, PLoS ONE, 17,

425 e0278 584, https://doi.org/10.1371/journal.pone.0278584, 2022a.

Belviso, S., Remaud, M., Abadie, C., Maignan, F., Ramonet, M., and Peylin, P.: Ongoing Decline in the Atmospheric COS Seasonal Cycle Amplitude over Western Europe: Implications for Surface Fluxes, Atmosphere, 13, 812, https://doi.org/10.3390/atmos13050812, 2022b.

Belviso, S., Pison, I., Petit, J.-E., Berchet, A., Remaud, M., Simon, L., Ramonet, M., Delmotte, M., Kazan, V., Yver-Kwok, C., and Lopez, M.: The Z-2018 emissions inventory of COS in Europe: A semiquantitative multi-data-streams evaluation, Atmospheric Environment,

430 300, 119 689, https://doi.org/10.1016/j.atmosenv.2023.119689, 2023.

Berchet, A., Sollum, E., Pison, I., Thompson, R. L., Thanwerdas, J., Fortems-Cheiney, A., Peet, J. C. A. v., Potier, E., Chevallier, F., Broquet, G., and Adrien, B.: The Community Inversion Framework: codes and documentation, https://doi.org/10.5281/zenodo.5045730, 2021.

Berchet, A., Pison, I., and Narbaud, C.: FLEXPART-GUI-toolbox, https://doi.org/10.5281/zenodo.7766372, 2023.

Berry, J., Wolf, A., Campbell, J. E., Baker, I., Blake, N., Blake, D., Denning, A. S., Kawa, S. R., Montzka, S. A., Seibt, U., Stim-

435 ler, K., Yakir, D., and Zhu, Z.: A coupled model of the global cycles of carbonyl sulfide and CO2: A possible new window on the carbon cycle, Journal of Geophysical Research: Biogeosciences, 118, 842–852, https://doi.org/10.1002/jgrg.20068, _eprint: https://onlinelibrary.wiley.com/doi/pdf/10.1002/jgrg.20068, 2013.

Bloem, E., Haneklaus, S., Kesselmeier, J., and Schnug, E.: Sulfur Fertilization and Fungal Infections Affect the Exchange of H2S and COS from Agricultural Crops, Journal of Agricultural and Food Chemistry, 60, 7588–7596, https://doi.org/10.1021/jf301912h, 2012.

440 Brownlee, B. G., Kenefick, S. L., MacInnis, G. A., and Hrudey, S. E.: Characterization of odorous compounds from bleached kraft pulp mill effluent, Water Science and Technology, 31, 35–40, https://doi.org/10.1016/0273-1223(95)00453-T, 1995.

Campbell, J. E., Berry, J. A., Seibt, U., Smith, S. J., Montzka, S. A., Launois, T., Belviso, S., Bopp, L., and Laine, M.: Large historical growth in global terrestrial gross primary production, Nature, 544, 84–87, https://doi.org/10.1038/nature22030, publisher: Nature Publishing Group, 2017.

445 Chen, J.: Chapter 4 - Synthetic Textile Fibers: Regenerated Cellulose Fibers, in: Textiles and Fashion, edited by Sinclair, R., Woodhead Publishing Series in Textiles, pp. 79–95, Woodhead Publishing, ISBN 978-1-84569-931-4, https://doi.org/10.1016/B978-1-84569-931-4.00004-0, 2015.

Cheremisinoff, N. P. and Rosenfeld, P. E.: Chapter 6 - Sources of air emissions from pulp and paper mills, in: Handbook of Pollution Prevention and Cleaner Production, edited by Cheremisinoff, N. P. and Rosenfeld, P. E., pp. 179–259, William Andrew Publishing,

450 Oxford, ISBN 978-0-08-096446-1, https://doi.org/https://doi.org/10.1016/B978-0-08-096446-1.10006-1, 2010.

Chin, M. and Davis, D. D.: Global sources and sinks of OCS and CS2 and their distributions, Global Biogeochemical Cycles, 7, 321–337, https://doi.org/10.1029/93GB00568, _eprint: https://onlinelibrary.wiley.com/doi/pdf/10.1029/93GB00568, 1993.

Commane, R., Meredith, L. K., Baker, I. T., Berry, J. A., Munger, J. W., Montzka, S. A., Templer, P. H., Juice, S. M., Zahniser, M. S., and Wofsy, S. C.: Seasonal fluxes of carbonyl sulfide in a midlatitude forest, Proceedings of the National Academy of Sciences, 112,

455 14 162–14 167, https://doi.org/10.1073/pnas.1504131112, publisher: Proceedings of the National Academy of Sciences, 2015.

DiMario, R. J., Quebedeaux, J. C., Longstreth, D. J., Dassanayake, M., Hartman, M. M., and Moroney, J. V.: The Cytoplasmic Carbonic Anhydrases βCA2 and βCA4 Are Required for Optimal Plant Growth at Low CO2, Plant Physiol, 171, 280–293, https://doi.org/10.1104/pp.15.01990, 2016.

Du, Q., Mu, Y., Zhang, C., Liu, J., Zhang, Y., and Liu, C.: Photochemical production of carbonyl sulfide, carbon disulfide and dimethyl

460 sulfide in a lake water, Journal of Environmental Sciences, 51, 146–156, https://doi.org/10.1016/j.jes.2016.08.006, 2017.

Harnisch, J., Borchers, R., and Fabian, P.: COS, CS2 and SO2 in aluminium smelter exhaust, Environ. Sci. & Pollut. Res., 2, 229–232, https://doi.org/10.1007/BF02986771, 1995.

Haynes, K. D., Baker, I. T., Denning, A. S., Stöckli, R., Schaefer, K., Lokupitiya, E. Y., and Haynes, J. M.: Representing Grasslands Using Dynamic Prognostic Phenology Based on Biological Growth Stages: 1. Implementation in the Simple Biosphere

465 Model (SiB4), Journal of Advances in Modeling Earth Systems, 11, 4423–4439, https://doi.org/10.1029/2018MS001540, _eprint: https://onlinelibrary.wiley.com/doi/pdf/10.1029/2018MS001540, 2019a.

Haynes, K. D., Baker, I. T., Denning, A. S., Wolf, S., Wohlfahrt, G., Kiely, G., Minaya, R. C., and Haynes, J. M.: Representing Grasslands Using Dynamic Prognostic Phenology Based on Biological Growth Stages: Part 2. Carbon Cycling, Journal of Advances in Modeling Earth Systems, 11, 4440–4465, https://doi.org/10.1029/2018MS001541, _eprint:

470 https://onlinelibrary.wiley.com/doi/pdf/10.1029/2018MS001541, 2019b.

Hersbach, H., Bell, B., Berrisford, P., Hirahara, S., Horányi, A., Muñoz-Sabater, J., Nicolas, J., Peubey, C., Radu, R., Schepers, D., Simmons, A., Soci, C., Abdalla, S., Abellan, X., Balsamo, G., Bechtold, P., Biavati, G., Bidlot, J., Bonavita, M., De Chiara, G., Dahlgren, P., Dee, D., Diamantakis, M., Dragani, R., Flemming, J., Forbes, R., Fuentes, M., Geer, A., Haimberger, L., Healy, S., Hogan, R. J., Hólm, E., Janisková, M., Keeley, S., Laloyaux, P., Lopez, P., Lupu, C., Radnoti, G., de Rosnay, P., Rozum, I., Vamborg, F., Vil-

475   laume, S., and Thépaut, J.-N.: The ERA5 global reanalysis, Quarterly Journal of the Royal Meteorological Society, 146, 1999–2049, https://doi.org/10.1002/qj.3803, _eprint: https://onlinelibrary.wiley.com/doi/pdf/10.1002/qj.3803, 2020.

Hilton, T. W., Zumkehr, A., Kulkarni, S., Berry, J., Whelan, M. E., and Campbell, J. E.: Large variability in ecosystem models explains uncertainty in a critical parameter for quantifying GPP with carbonyl sulphide, Tellus B: Chemical and Physical Meteorology, 67, https://doi.org/10.3402/tellusb.v67.26329, 2015.

480   Hilton, T. W., Whelan, M. E., Zumkehr, A., Kulkarni, S., Berry, J. A., Baker, I. T., Montzka, S. A., Sweeney, C., Miller, B. R., and Elliott Campbell, J.: Peak growing season gross uptake of carbon in North America is largest in the Midwest USA, Nature Clim Change, 7, 450–454, https://doi.org/10.1038/nclimate3272, publisher: Nature Publishing Group, 2017.

Kamezaki, K., Danielache, S. O., Ishidoya, S., Maeda, T., and Murayama, S.: Development of compact continuous measurement system for atmospheric carbonyl sulfide concentration, Atmospheric Measurement Techniques Discussions, pp. 1–22, https://doi.org/10.5194/amt-

485   2023-209, publisher: Copernicus GmbH, 2023.

Kettle, A. J., Kuhn, U., von Hobe, M., Kesselmeier, J., and Andreae, M. O.: Global budget of atmospheric carbonyl sulfide: Temporal and spatial variations of the dominant sources and sinks, Journal of Geophysical Research: Atmospheres, 107, ACH 25–1–ACH 25–16, https://doi.org/10.1029/2002JD002187, _eprint: https://onlinelibrary.wiley.com/doi/pdf/10.1029/2002JD002187, 2002.

Khalil, M. A. K. and Rasmussen, R. A.: Global sources, lifetimes and mass balances of carbonyl sulfide (OCS) and carbon disulfide (CS2)

490   in the earth's atmosphere, Atmospheric Environment (1967), 18, 1805–1813, https://doi.org/10.1016/0004-6981(84)90356-1, 1984.

Kitz, F., Gerdel, K., Hammerle, A., Laterza, T., Spielmann, F. M., and Wohlfahrt, G.: In situ soil COS exchange of a temperate mountain grassland under simulated drought, Oecologia, 183, 851–860, https://doi.org/10.1007/s00442-016-3805-0, 2017.

Kitz, F., Spielmann, F. M., Hammerle, A., Kolle, O., Migliavacca, M., Moreno, G., Ibrom, A., Krasnov, D., Noe, S. M., and Wohlfahrt, G.: Soil COS Exchange: A Comparison of Three European Ecosystems, Global Biogeochemical Cycles, 34, e2019GB006 202,

495   https://doi.org/10.1029/2019GB006202, _eprint: https://onlinelibrary.wiley.com/doi/pdf/10.1029/2019GB006202, 2020.

Kooijmans, L. M. J., Uitslag, N. A. M., Zahniser, M. S., Nelson, D. D., Montzka, S. A., and Chen, H.: Continuous and high-precision atmospheric concentration measurements of COS, CO_2, CO and H_2O using a quantum cascade laser spectrometer (QCLS), Atmospheric Measurement Techniques, 9, 5293–5314, https://doi.org/10.5194/amt-9-5293-2016, publisher: Copernicus GmbH, 2016.

Kooijmans, L. M. J., Cho, A., Ma, J., Kaushik, A., Haynes, K. D., Baker, I., Luijkx, I. T., Groenink, M., Peters, W., Miller, J. B., Berry, J. A.,

500   Ogée, J., Meredith, L. K., Sun, W., Kohonen, K.-M., Vesala, T., Mammarella, I., Chen, H., Spielmann, F. M., Wohlfahrt, G., Berkelhammer, M., Whelan, M. E., Maseyk, K., Seibt, U., Commane, R., Wehr, R., and Krol, M.: Evaluation of carbonyl sulfide biosphere exchange in the Simple Biosphere Model (SiB4), Biogeosciences, 18, 6547–6565, https://doi.org/10.5194/bg-18-6547-2021, 2021a.

Kooijmans, L. M. J., Cho, A., Ma, J., Kaushik, A., Haynes, K. D., Baker, I., Luijkx, I. T., Groenink, M., Peters, W., Miller, J. B., Berry, J. A., Ogée, J., Meredith, L. K., Sun, W., Kohonen, K.-M., Vesala, T., Mammarella, I., Chen, H., Spielmann, F. M., Wohlfahrt, G., Berkelhammer,

505   M., Whelan, M. E., Maseyk, K., Seibt, U., Commane, R., Wehr, R., and Krol, M.: Evaluation of carbonyl sulfide biosphere exchange in the Simple Biosphere Model (SiB4), Biogeosciences, 18, 6547–6565, https://doi.org/10.5194/bg-18-6547-2021, publisher: Copernicus GmbH, 2021b.

Krinner, G., Viovy, N., de Noblet-Ducoudré, N., Ogée, J., Polcher, J., Friedlingstein, P., Ciais, P., Sitch, S., and Prentice, I. C.: A dynamic global vegetation model for studies of the coupled atmosphere-biosphere system, Global Biogeochemical Cycles, 19,

510   https://doi.org/https://doi.org/10.1029/2003GB002199, 2005.

Kuai, L., Worden, J. R., Campbell, J. E., Kulawik, S. S., Li, K.-F., Lee, M., Weidner, R. J., Montzka, S. A., Moore, F. L., Berry, J. A., Baker, I., Denning, A. S., Bian, H., Bowman, K. W., Liu, J., and Yung, Y. L.: Estimate of carbonyl sulfide tropical oceanic surface fluxes

using Aura Tropospheric Emission Spectrometer observations, Journal of Geophysical Research: Atmospheres, 120, 11,012–11,023, https://doi.org/10.1002/2015JD023493, _eprint: https://onlinelibrary.wiley.com/doi/pdf/10.1002/2015JD023493, 2015.

515 Launois, T., Peylin, P., Belviso, S., and Poulter, B.: A new model of the global biogeochemical cycle of carbonyl sulfide – Part 2: Use of carbonyl sulfide to constrain gross primary productivity in current vegetation models, Atmospheric Chemistry and Physics, 15, 9285–9312, https://doi.org/10.5194/acp-15-9285-2015, publisher: Copernicus GmbH, 2015.

Lennartz, S. T., Marandino, C. A., von Hobe, M., Cortes, P., Quack, B., Simo, R., Booge, D., Pozzer, A., Steinhoff, T., Arevalo-Martinez, D. L., Kloss, C., Bracher, A., Röttgers, R., Atlas, E., and Krüger, K.: Direct oceanic emissions unlikely to account for the missing source

520 of atmospheric carbonyl sulfide, Atmospheric Chemistry and Physics, 17, 385–402, https://doi.org/10.5194/acp-17-385-2017, publisher: Copernicus GmbH, 2017.

Lennartz, S. T., Gauss, M., von Hobe, M., and Marandino, C. A.: Monthly resolved modelled oceanic emissions of carbonyl sulphide and carbon disulphide for the period 2000–2019, Earth System Science Data, 13, 2095–2110, https://doi.org/10.5194/essd-13-2095-2021, publisher: Copernicus GmbH, 2021.

525 Ma, J., Kooijmans, L. M. J., Cho, A., Montzka, S. A., Glatthor, N., Worden, J. R., Kuai, L., Atlas, E. L., and Krol, M. C.: Inverse modelling of carbonyl sulfide: implementation, evaluation and implications for the global budget, Atmospheric Chemistry and Physics, 21, 3507–3529, https://doi.org/10.5194/acp-21-3507-2021, publisher: Copernicus GmbH, 2021.

Ma, J., Remaud, M., Peylin, P., Patra, P., Niwa, Y., Rodenbeck, C., Cartwright, M., Harrison, J. J., Chipperfield, M. P., Pope, R. J., Wilson, C., Belviso, S., Montzka, S. A., Vimont, I., Moore, F., Atlas, E. L., Schwartz, E., and Krol, M. C.: Intercomparison of At-

530 mospheric Carbonyl Sulfide (TransCom-COS): 2. Evaluation of Optimized Fluxes Using Ground-Based and Aircraft Observations, Journal of Geophysical Research: Atmospheres, 128, e2023JD039 198, https://doi.org/https://doi.org/10.1029/2023JD039198, _eprint: https://agupubs.onlinelibrary.wiley.com/doi/pdf/10.1029/2023JD039198, 2023.

Maignan, F., Abadie, C., Remaud, M., Kooijmans, L. M. J., Kohonen, K.-M., Commane, R., Wehr, R., Campbell, J. E., Belviso, S., Montzka, S. A., Raoult, N., Seibt, U., Shiga, Y. P., Vuichard, N., Whelan, M. E., and Peylin, P.: Carbonyl sulfide: comparing a mechanistic rep-

535 resentation of the vegetation uptake in a land surface model and the leaf relative uptake approach, Biogeosciences, 18, 2917–2955, https://doi.org/10.5194/bg-18-2917-2021, publisher: Copernicus GmbH, 2021.

Masaki, Y., Iizuka, R., Kato, H., Kojima, Y., Ogawa, T., Yoshida, M., Matsushita, Y., and Katayama, Y.: Fungal Carbonyl Sulfide Hydrolase of Trichoderma harzianum Strain THIF08 and Its Relationship with Clade D β-Carbonic Anhydrases, Microbes Environ, 36, ME20 058, https://doi.org/10.1264/jsme2.ME20058, 2021.

540 Maseyk, K., Berry, J. A., Billesbach, D., and Seibt, U.: Sources and sinks of carbonyl sulfide in an agricultural field in the Southern Great Plains, P. Natl. Acad. Sci. USA, 111, https://doi.org/10.1073/pnas.1319132111, 2014.

Mihalopoulos, N., Nguyen, B. C., Putaud, J. P., and Belviso, S.: The oceanic source of carbonyl sulfide (COS), Atmospheric Environment. Part A. General Topics, 26, 1383–1394, https://doi.org/10.1016/0960-1686(92)90123-3, 1992.

Montzka, S. A., Calvert, P., Hall, B. D., Elkins, J. W., Conway, T. J., Tans, P. P., and Sweeney, C.: On the global distribution, seasonality,

545 and budget of atmospheric carbonyl sulfide (COS) and some similarities to CO2, Journal of Geophysical Research: Atmospheres, 112, https://doi.org/10.1029/2006JD007665, _eprint: https://onlinelibrary.wiley.com/doi/pdf/10.1029/2006JD007665, 2007.

Ogée, J., Sauze, J., Kesselmeier, J., Genty, B., Van Diest, H., Launois, T., and Wingate, L.: A new mechanistic framework to predict OCS fluxes from soils, Biogeosciences, 13, 2221–2240, https://doi.org/10.5194/bg-13-2221-2016, publisher: Copernicus GmbH, 2016.

Pisso, I., Sollum, E., Grythe, H., Kristiansen, N. I., Cassiani, M., Eckhardt, S., Arnold, D., Morton, D., Thompson, R. L., Groot Zwaaftink,

550 C. D., Evangeliou, N., Sodemann, H., Haimberger, L., Henne, S., Brunner, D., Burkhart, J. F., Fouilloux, A., Brioude, J., Philipp, A.,

Seibert, P., and Stohl, A.: The Lagrangian particle dispersion model FLEXPART version 10.4, Geoscientific Model Development, 12, 4955–4997, https://doi.org/https://doi.org/10.5194/gmd-12-4955-2019, publisher: Copernicus GmbH, 2019.

Protoschill-Krebs, G., Wilhelm, C., and Kesselmeier, J.: Consumption of carbonyl sulphide (COS) by higher plant carbonic anhydrase (CA), Atmospheric Environment, 30, 3151–3156, https://api.semanticscholar.org/CorpusID:84856936, 1996.

555 Ramonet, M., Ciais, P., Rivier, L., Laurila, T., Vermeulen, A., Geever, M., Jordan, A., Levin, I., Laurent, O., Delmotte, M., Wastine, B., Hazan, L., Schmidt, M., Tarniewicz, J., Vuillemin, C., Pison, I., Spain, G., and Paris, J.-D.: The ICOS Atmospheric Thematic Center (ATC), GAW Report No. 206, 16th WMO/IAEA Meeting on Carbon Dioxide, Other Greenhouse Gases and Related Tracers Measurement Techniques (GGMT-2011), 2011.

Remaud, M., Chevallier, F., Maignan, F., Belviso, S., Berchet, A., Parouffe, A., Abadie, C., Bacour, C., Lennartz, S., and Peylin, P.: Plant
560 gross primary production, plant respiration and carbonyl sulfide emissions over the globe inferred by atmospheric inverse modelling, Atmospheric Chemistry and Physics, 22, 2525–2552, https://doi.org/10.5194/acp-22-2525-2022, publisher: Copernicus GmbH, 2022.

Remaud, M., Ma, J., Krol, M., Abadie, C., Cartwright, M. P., Patra, P., Niwa, Y., Rodenbeck, C., Belviso, S., Kooijmans, L., Lennartz, S., Maignan, F., Chevallier, F., Chipperfield, M. P., Pope, R. J., Harrison, J. J., Vimont, I., Wilson, C., and Peylin, P.: Intercomparison of Atmospheric Carbonyl Sulfide (TransCom-COS; Part One): Evaluating the Impact of Transport and Emissions on Tro-
565 pospheric Variability Using Ground-Based and Aircraft Data, Journal of Geophysical Research: Atmospheres, 128, e2022JD037 817, https://doi.org/https://doi.org/10.1029/2022JD037817, 2023.

Sandoval-Soto, L., Stanimirov, M., Hobe, M. v., Schmitt, V., Valdes, J., Wild, A., and Kesselmeier, J.: Global uptake of carbonyl sulfide (COS) by terrestrial vegetation: Estimates corrected by deposition velocities normalized to the uptake of carbon dioxide (CO_2), Biogeosciences, 2, 125–132, https://api.semanticscholar.org/CorpusID:16099750, 2005.

570 Sarwar, G., Kang, D., Henderson, B. H., Hogrefe, C., Appel, W., and Mathur, R.: Examining the Impact of Dimethyl Sulfide Emissions on Atmospheric Sulfate over the Continental U.S., Atmosphere, 14, 660, https://doi.org/10.3390/atmos14040660, number: 4 Publisher: Multidisciplinary Digital Publishing Institute, 2023.

Seibert, P. and Frank, A.: Source-receptor matrix calculation with a Lagrangian particle dispersion model in backward mode, Atmospheric Chemistry and Physics, 4, 51–63, https://doi.org/10.5194/acp-4-51-2004, 2004.

575 Stickel, R. E., Chin, M., Daykin, E. P., Hynes, A. J., Wine, P. H., and Wallington, T. J.: Mechanistic studies of the hydroxyl-initiated oxidation of carbon disulfide in the presence of oxygen, The Journal of Physical Chemistry, 97, 13 653–13 661, https://doi.org/10.1021/j100153a038, publisher: American Chemical Society, 1993.

Stinecipher, J., Cameron-Smith, P., Blake, N., Kuai, L., Lejeune, B., Mahieu, E., Simpson, I., and Campbell, J.: Biomass Burning Unlikely to Account for Missing Source of Carbonyl Sulfide, Geophysical Research Letters, 46, 14 912–14 920,
580 https://doi.org/10.1029/2019GL085567, _eprint: https://onlinelibrary.wiley.com/doi/pdf/10.1029/2019GL085567, 2019.

Stohl, A., Forster, C., Frank, A., Seibert, P., Wotawa, G., et al.: Technical note: The Lagrangian particle dispersion model FLEXPART version 6.2, Atmos. Chem. Phys., 5, 2461–2474, http://hal-insu.archives-ouvertes.fr/hal-00301615/, 2005.

Suntharalingam, P., Kettle, A. J., Montzka, S. M., and Jacob, D. J.: Global 3-D model analysis of the seasonal cycle of atmospheric carbonyl sulfide: Implications for terrestrial vegetation uptake, Geophysical Research Letters, 35, https://doi.org/10.1029/2008GL034332, _eprint:
585 https://onlinelibrary.wiley.com/doi/pdf/10.1029/2008GL034332, 2008.

Thompson, R. L. and Stohl, A.: FLEXINVERT: an atmospheric Bayesian inversion framework for determining surface fluxes of trace species using an optimized grid, Geoscientific Model Development, 7, 2223–2242, https://doi.org/10.5194/gmd-7-2223-2014, publisher: Copernicus GmbH, 2014.

Tipka, A., Haimberger, L., and Seibert, P.: Flex_extract v7.1.2 – a software package to retrieve and prepare ECMWF data for use in FLEX-PART, Geoscientific Model Development, 13, 5277–5310, https://doi.org/10.5194/gmd-13-5277-2020, publisher: Copernicus GmbH, 2020.

von Hobe, M., Taraborrelli, D., Alber, S., Bohn, B., Dorn, H.-P., Fuchs, H., Li, Y., Qiu, C., Rohrer, F., Sommariva, R., Stroh, F., Tan, Z., Wedel, S., and Novelli, A.: Measurement report: Carbonyl sulfide production during dimethyl sulfide oxidation in the atmospheric simulation chamber SAPHIR, Atmospheric Chemistry and Physics, 23, 10 609–10 623, https://doi.org/10.5194/acp-23-10609-2023, publisher: Copernicus GmbH, 2023.

Water, U. S. E. P. A. O. o.: Preliminary Study of Carbon Disulfide Discharges from Cellulose Products Manufacturers, Tech. Rep. 821-R-11-009, United States Environmental Protection Agency, https://www.epa.gov/sites/production/files/2015-10/documents/cellulose-products_prelimstudy_2011.pdf, 2011.

Whelan, M., Lennartz, S., Gimeno, T., Wehr, R., Wohlfahrt, G., Wang, Y., Kooijmans, L., Hilton, T., Belviso, S., Peylin, P., Commane, R., Sun, W., Chen, H., Kuai, L., Mammarella, I., Maseyk, K., Berkelhammer, M., Li, K.-F., Yakir, D., Zumkehr, A., Katayama, Y., Ogée, J., Spielmann, F., Kitz, F., Rastogi, B., Kesselmeier, J., Marshall, J., Erkkilä, K.-M., Wingate, L., Meredith, L., He, W., Bunk, R., Launois, T., Vesala, T., Schmidt, J., Fichot, C. G., Seibt, U., Saleska, S., Saltzman, E., Montzka, S., Berry, J., and Campbell, J. E.: Reviews and syntheses: Carbonyl sulfide as a multi-scale tracer for carbon and water cycles, Biogeosciences, 15, 3625, https://doi.org/10.5194/bg-15-3625-2018, 2018.

Whelan, M. E. and Rhew, R. C.: Carbonyl sulfide produced by abiotic thermal and photodegradation of soil organic matter from wheat field substrate, Journal of Geophysical Research: Biogeosciences, 120, 54–62, https://doi.org/10.1002/2014JG002661, _eprint: https://onlinelibrary.wiley.com/doi/pdf/10.1002/2014JG002661, 2015.

Whelan, M. E., Hilton, T. W., Berry, J. A., Berkelhammer, M., Desai, A. R., and Campbell, J. E.: Carbonyl sulfide exchange in soils for better estimates of ecosystem carbon uptake, Atmospheric Chemistry and Physics, 16, 3711–3726, https://doi.org/10.5194/acp-16-3711-2016, publisher: Copernicus GmbH, 2016.

Zanchetta, A., Kooijmans, L. M. J., van Heuven, S., Scifo, A., Scheeren, H. A., Mammarella, I., Karstens, U., Ma, J., Krol, M., and Chen, H.: Sources and sinks of carbonyl sulfide inferred from tower and mobile atmospheric observations in the Netherlands, Biogeosciences, 20, 3539–3553, https://doi.org/10.5194/bg-20-3539-2023, publisher: Copernicus GmbH, 2023.

Zumkehr, A., Hilton, T. W., Whelan, M., Smith, S., Kuai, L., Worden, J., and Campbell, J. E.: Global gridded anthropogenic emissions inventory of carbonyl sulfide, Atmospheric Environment, 183, 11–19, https://doi.org/10.1016/j.atmosenv.2018.03.063, 2018.

Appendix A: Time series of observations and simulations
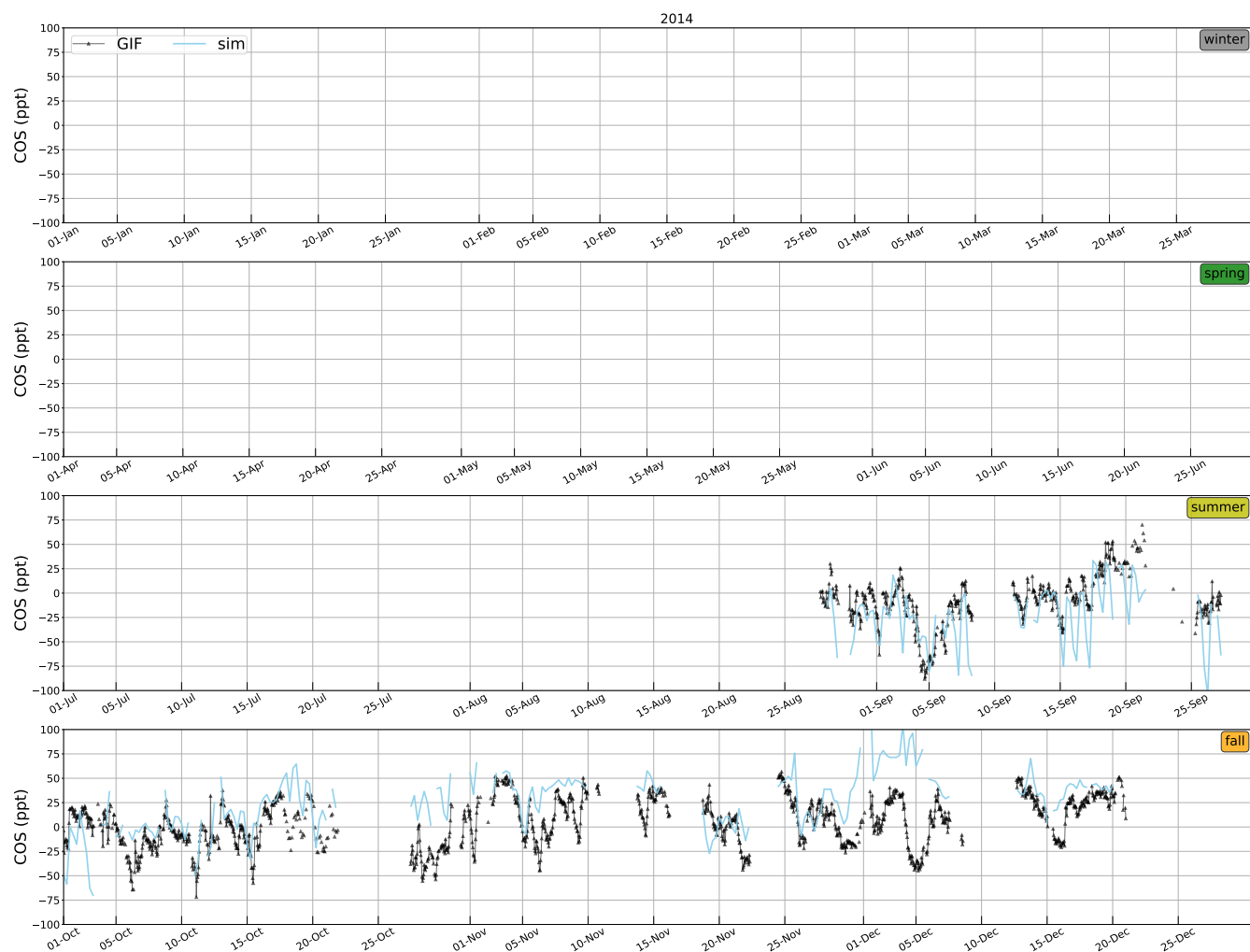
Figure A1. *Smoothed time series of observed and simulated atmospheric mixing ratios of COS at GIF in 2014. Observations are hourly averages; contributions taken into account in the simulations are the background + ocean + our home-made anthropogenic inventory + biogenic land with a monthly time-resolution for vegetation and soils (see Section 2.2 for details); smoothed by substracting the rolling 20-day mean of the observations to the observed and simulated time series. Note that the time series begins end of August 2014.*
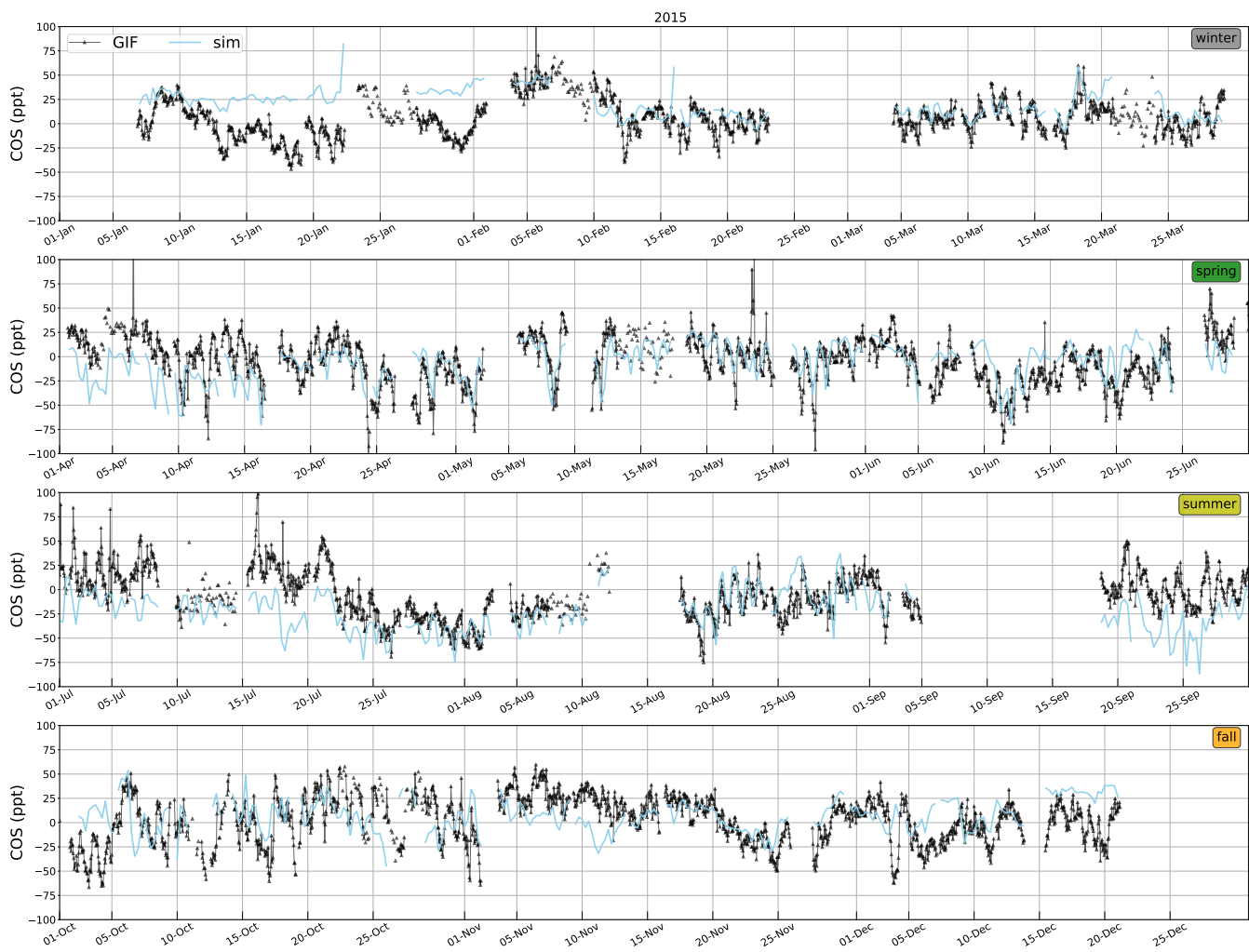
Figure A2. *Same as Fig. A1 for year 2015.*
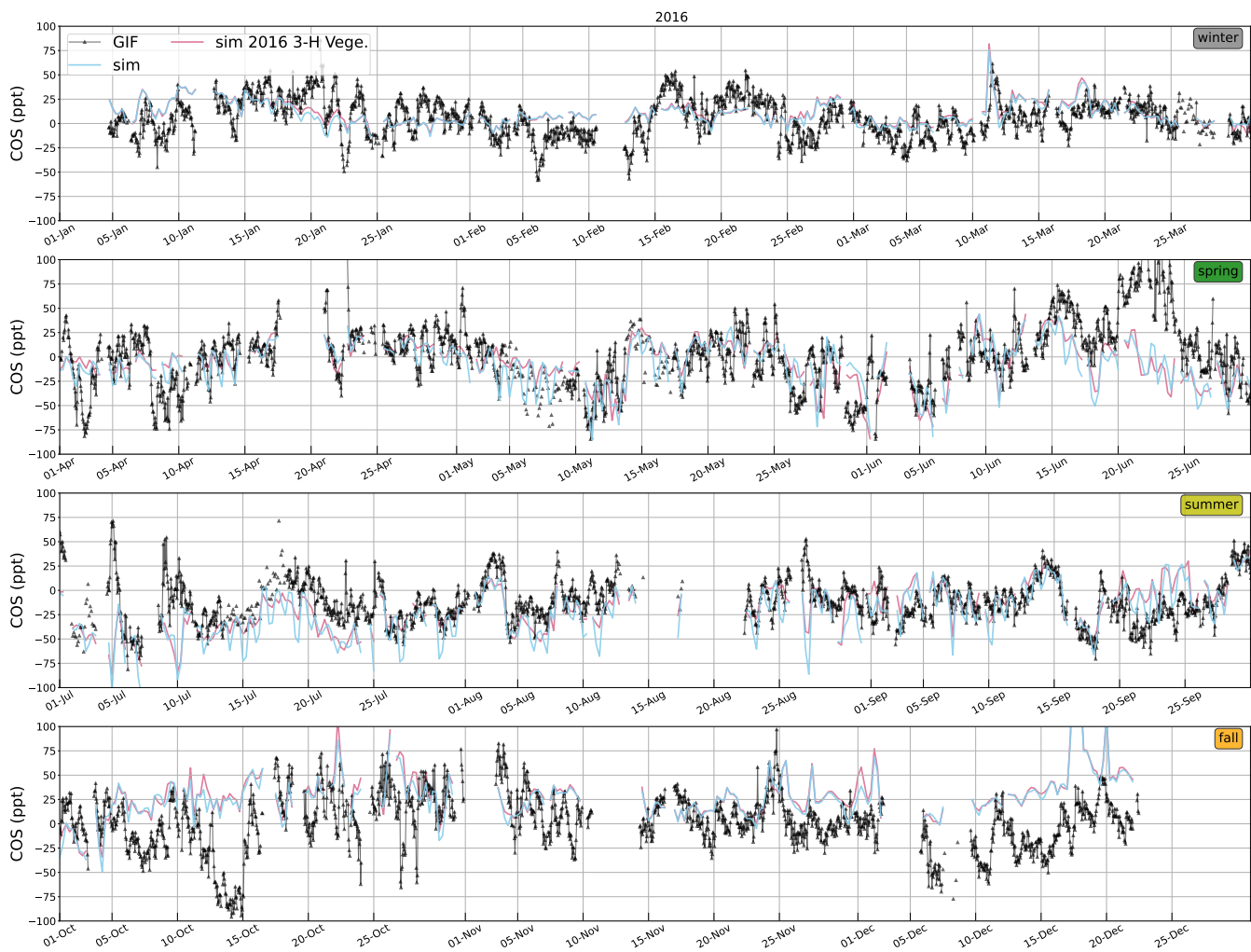
Figure A3. *Same as Fig. A1 for year 2016, with simulated contribution from the vegetation uptake with 3-hourly time-resolution (see Section 2.2 for details).*
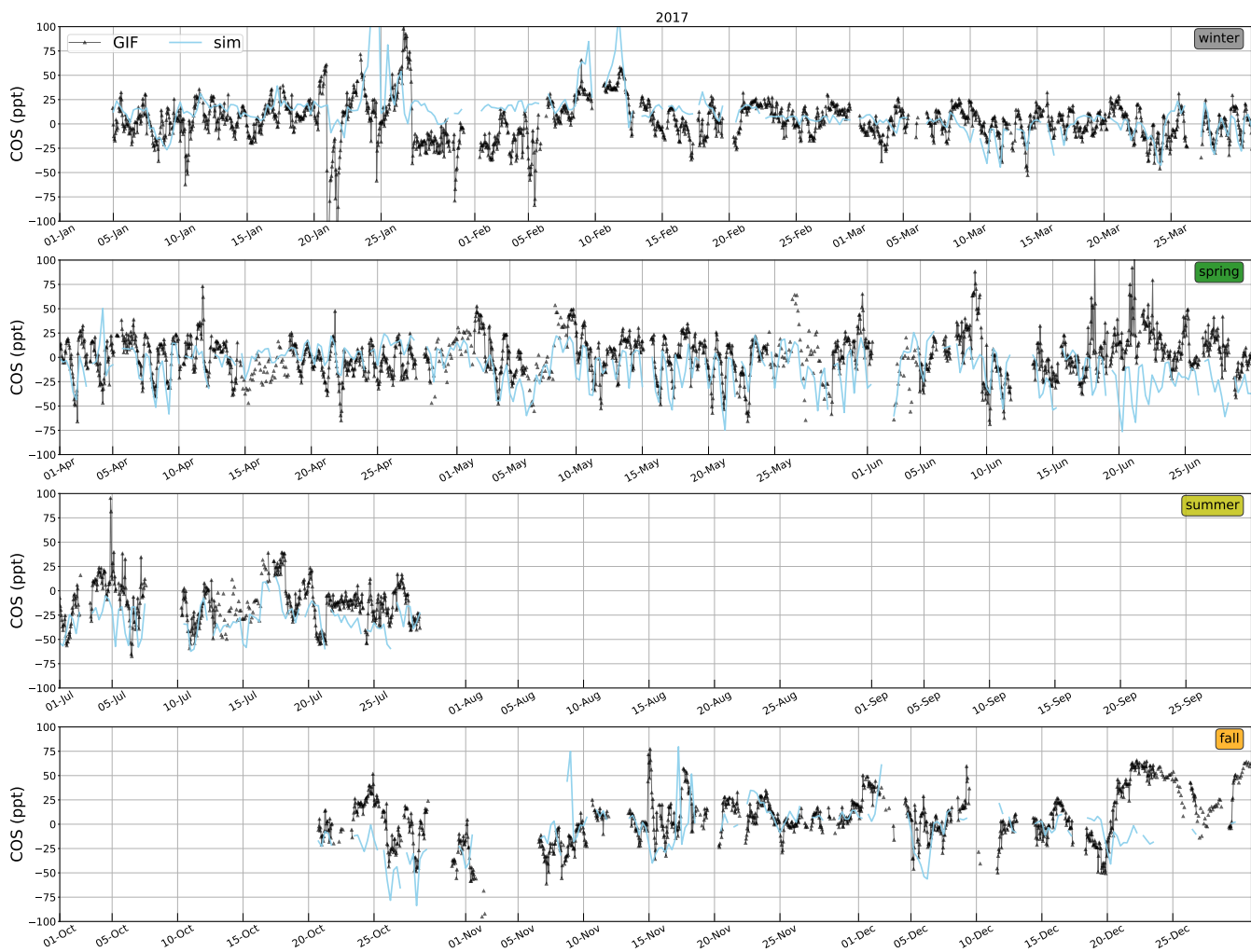
Figure A4. *Same as Fig. A1 for year 2017.*
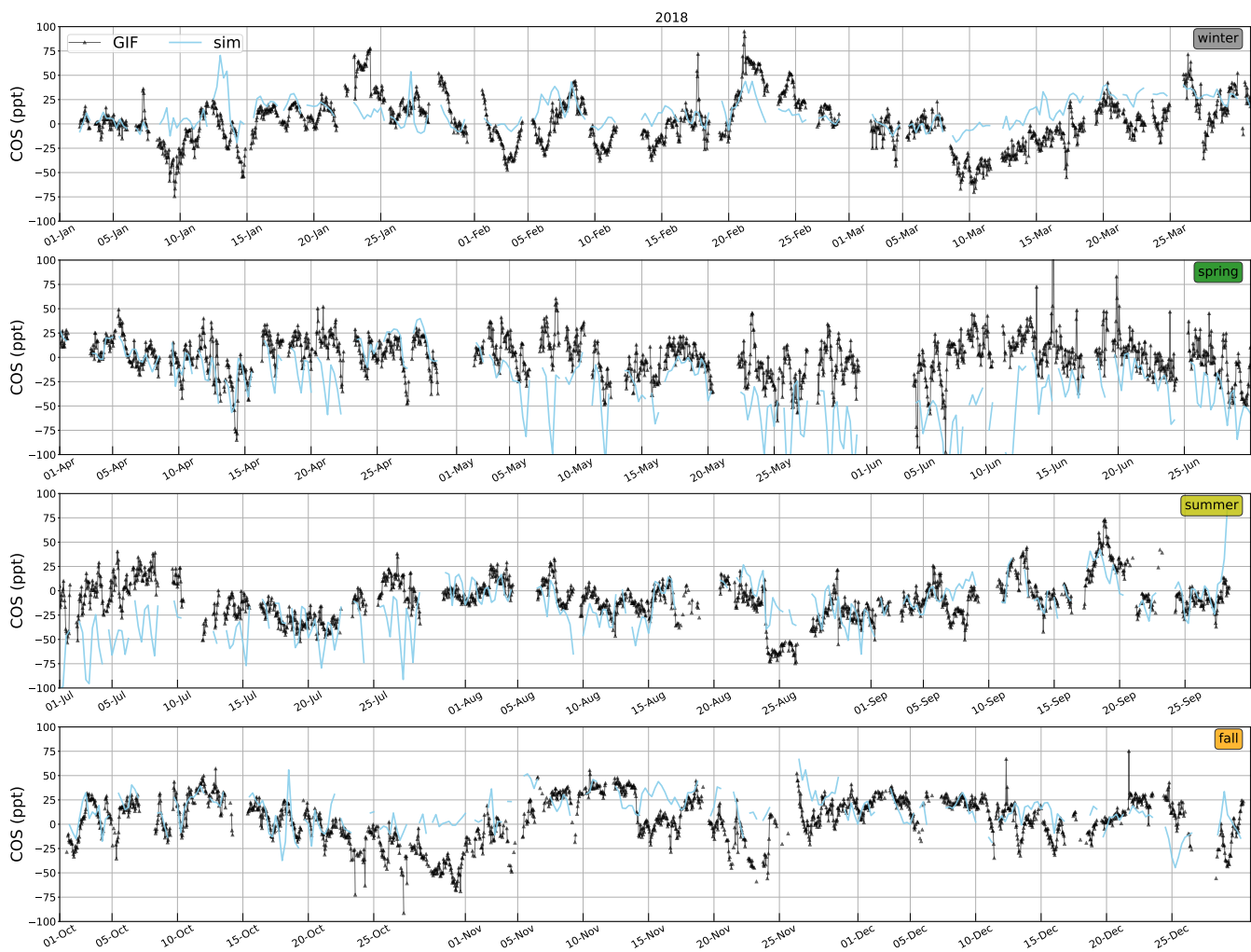
Figure A5. *Same as Fig. A1 for year 2018.*
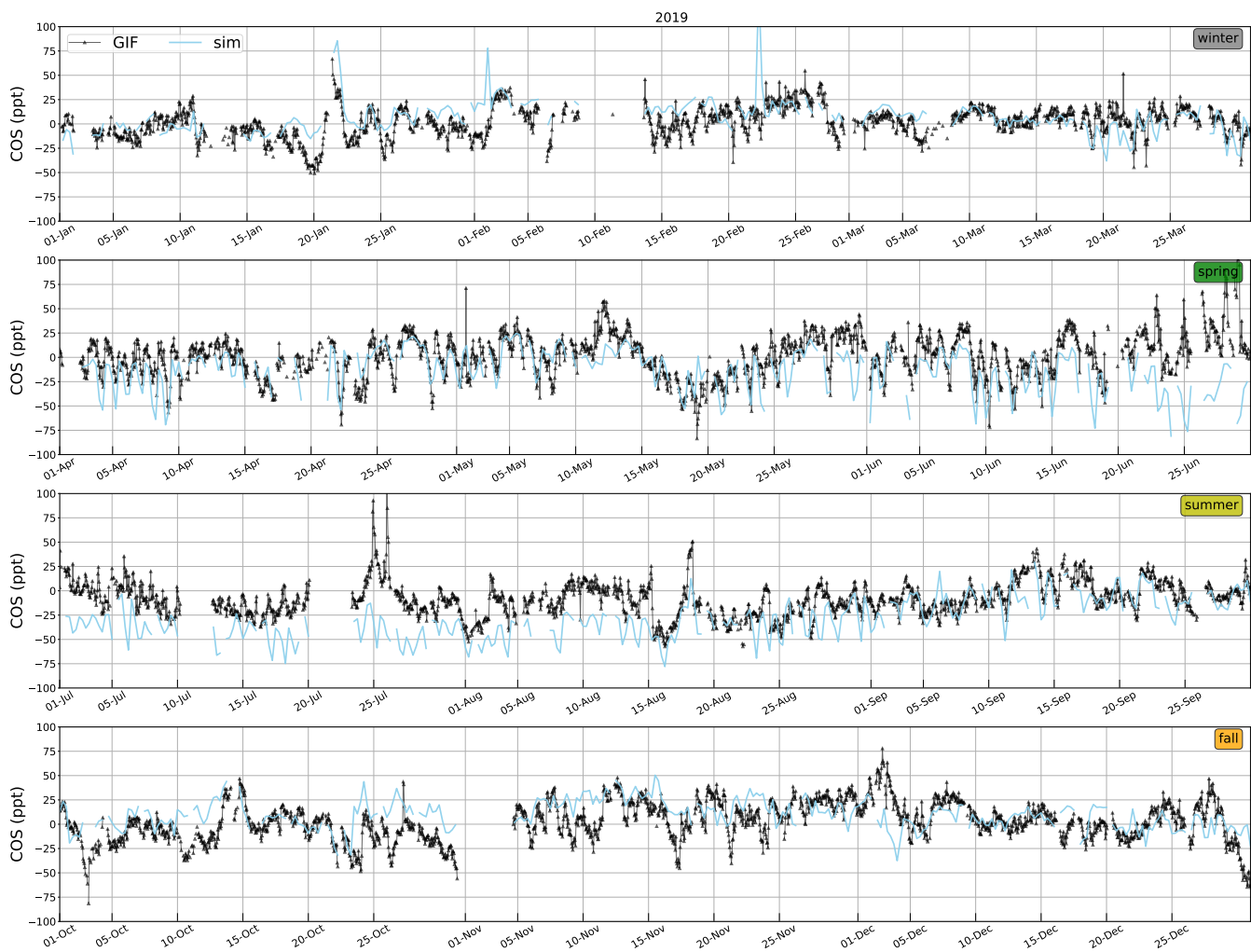
Figure A6. *Same as Fig. A1 for year 2019.*